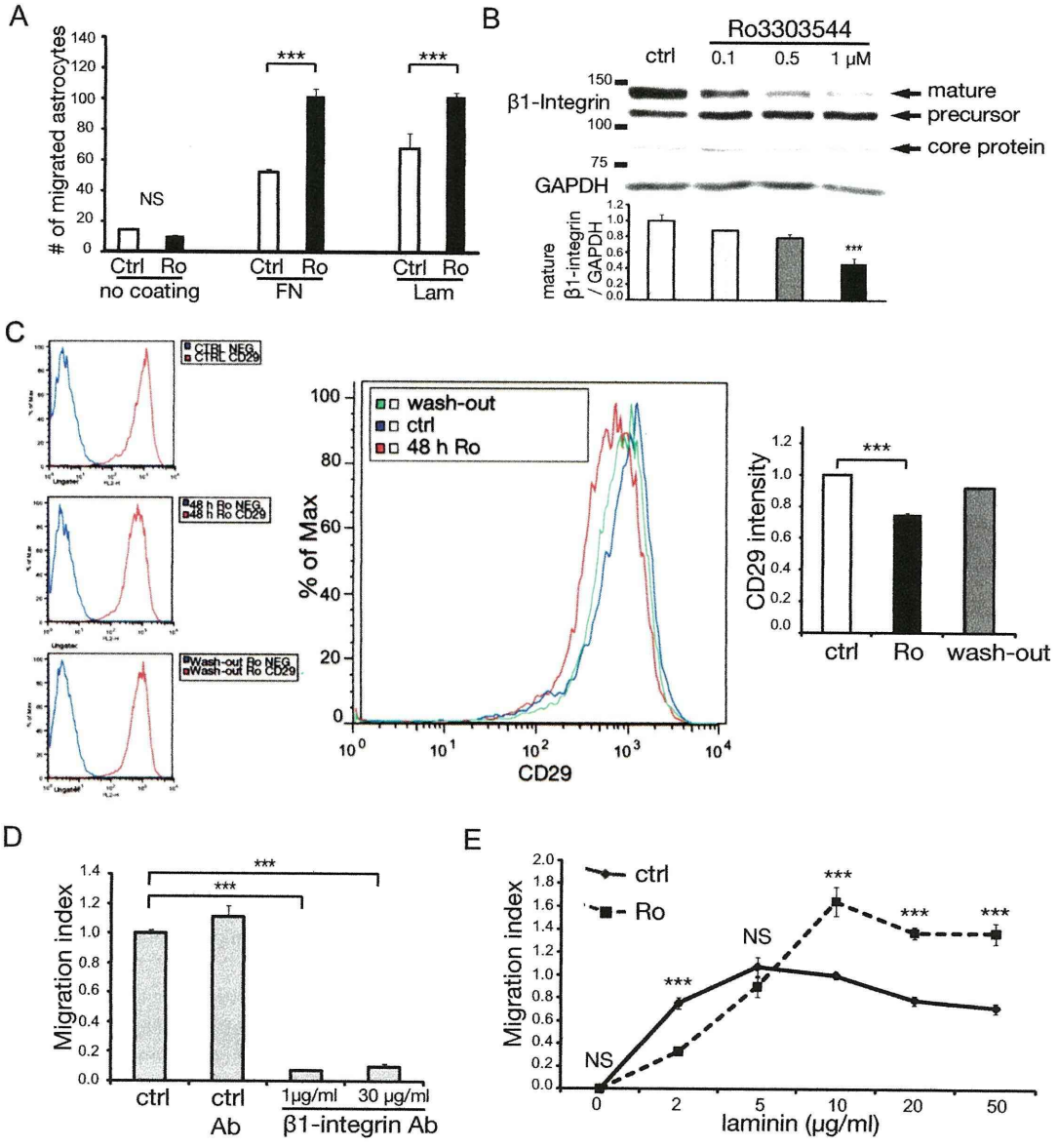


**Figure 8. Increased migration of astrocytes *in vitro* upon prolonged Ro3303544 treatment relies on reduced cell adhesion with the ECM due to decreased surface expression of β1-integrin.**

**A.** The pro-migratory effect of prolonged Ro3303544 treatment was similar on fibronectin and laminin. By contrast, migration of astrocytes in the absence of ECM coating was limited regardless of Ro3303544 treatment.

**B.** Treatment for 48 h with Ro3303544 dose-dependently decreased the expression level of mature β1-integrin in astrocytes. Histogram data represent mean ± SEM of a representative experiment performed in triplicate. $^{***}p < 0.001$.

**C.** Flow cytometric analysis confirmed that 48-h treatment with Ro3303544 decreased the cell-surface expression of β1-integrin on astrocytes. The specificity of the immunostaining is shown at left. CD29 = β1-integrin. A representative experiment is shown. $^{***}p < 0.001$, $n = 10\,000$ cells per sample (unpaired Student's *t*-test).

**D.** Migration assays using a function-blocking antibody against β1-integrin demonstrated that functional β1-integrin was required for the migration of the astrocytes.

**E.** The effect of Ro3303544 on *in vitro* astrocytes migration depended on the ECM concentration. While 48-h treatment with Ro3303544 resulted in decreased migration compared to control cells at low laminin concentrations, a pro-migratory effect was observed at higher concentrations. Data represent mean ± SD of three independent experiments. $^{***}p < 0.001$, $n = 9$.

as an example ECM protein, were examined following SCI. In control animals, while the expression of laminin was initially restricted to blood vessels at 4 and 7 DPI, its expression at the lesion epicentre was drastically upregulated from 10 DPI and maintained at 14 DPI (Fig 9A). The time course of laminin upregulation following injury was not affected by Ro3303544 treatment (not shown). Then, the effect of Ro3303544 administration on β1-integrin expression levels was evaluated *in vivo*. Although the pattern of the different forms of β1-integrin in spinal cord lysates was much more complex than in astrocytes *in vitro*, a significant decrease in the expression level of the higher molecular-weight β1-integrin band in the Ro3303544-treated mice was observed at 5 DPI (Fig 9B). Considering that laminin was upregulated only from 10 DPI, the expression level of β1-integrin was next examined at this time-point. The results showed β1-integrin remain significantly reduced in Ro3303544-treated mice at 10 DPI (Fig 9B).

Together, the observed Ro3303544-mediated reduction in β1-integrin expression in the spinal cord and the concomitant spontaneous upregulation of laminin at 10 DPI suggests that the mechanistic model proposed on the basis of the *in vitro* data is relevant *in vivo*.

## DISCUSSION

While the deleterious effects of reactive astrocytes and their associated glial scar after CNS injury are well established (Sofroniew, 2009), their beneficial roles have only been evidenced relatively recently (White & Jakeman, 2008). Using several conditional knock-out mice targeting STAT3 signalling in reactive astrocytes, we and others have previously observed that the compaction of inflammatory cells by migrating reactive astrocytes is associated with enhanced locomotor recovery after SCI (Herrmann et al, 2008; Okada et al, 2006). Here, we report that the pharmacological inhibition of GSK-3 using the novel, highly potent agent Ro3303544 successfully stimulated the migration of astrocytes both *in vitro* and *in vivo* and promoted functional recovery after SCI.

### GSK-3 and cell migration

Current data about the role of GSK-3 in cell migration are contradictory (Etienne-Manneville & Hall, 2003; Kapoor et al, 2008). Our observations demonstrate first that the effect of GSK-3 depends on the migration mode involved (interested readers are invited to read the extended discussion in Supporting Information). Although the *in vivo* pattern of endogenous astrocyte migration following CNS injury is unknown, glial cells migrate as single cells during development (Klambt, 2009). Moreover, the observed increased compaction of inflammatory cells *in vivo* after Ro3303544 administration (Fig 4) suggests that the migration of astrocytes observed in the single-cell transwell assay more closely resembles the situation of *in vivo* reactive astrocytes and reveals that the *in vitro* wound scratch assay is not always relevant to *in vivo* CNS injury.

### Mechanism of increased migration by the sustained inhibition of GSK-3

The historical model for describing the mesenchymal migration mode (DiMilla et al, 1991; Lauffenburger & Horwitz, 1996; Palecek et al, 1997) implies that cell migration speed depends on the strength of cell adhesion to the substratum. In agreement with the reduced surface expression of β1-integrin, the effect of Ro3303544 on migration was observed to depend on the

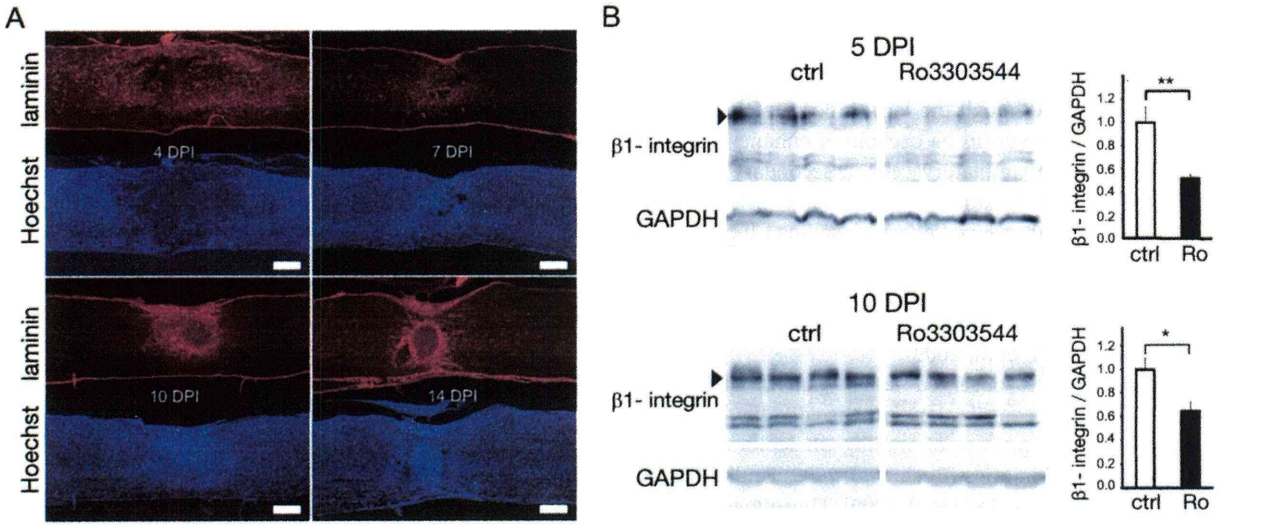


**Figure 9. The Ro3303544-mediated reduction of β1-integrin expression in the spinal cord is concomitant with the spontaneous upregulation of laminin at 10 DPI.**

**A.** Laminin was upregulated at 10 DPI in the lesion centre of the injured spinal cord. Red: laminin; blue: Hoechst nuclear staining. Scale bars, 500 μm.

**B.** At both 5 and 10 DPI, the higher-molecular-weight form of β1-integrin (arrowhead) was significantly decreased in the spinal cord of Ro3303544-treated mice compared to control mice. Data represent mean ± SEM. (**$p < 0.01$, *$p < 0.05$, unpaired t test, $n = 4$ mice per group and time-point.)

concentration of the laminin coating. The apparent discrepancy between the administration period of Ro3303544 *in vivo* (the first 5 days after injury) and the observation that the compaction of inflammatory cells increased compared to control at 14, but not 7 DPI suggests that the pro-migratory effect of Ro3303544 *in vivo* indeed depends on the spontaneous upregulation of ECM proteins following SCI, which we have demonstrated occurs at 10 DPI. Given the complexity of the lesion environment, as well as the number of molecules that potentially modulate the migration of reactive astrocytes, it seems plausible that the actual mechanism for the *in vivo* enhancement of migration by Ro3303544 is more complex than our proposed model.

### Mechanism of improved functional outcome by GSK-3 inhibition

The beneficial effect of GSK-3 inhibition in SCI using less potent and specific reagents has been previously reported (Cuzzocrea et al, 2006; Dill et al, 2008). This effect may involve reduced apoptosis and the direct promotion of axon outgrowth. While the direct stimulation of axon growth upon GSK-3 inhibition is still a matter of controversy in the literature (Alabed et al, 2010), we observed that Ro3303544 promoted the neurite outgrowth of embryonic hippocampal neurons *in vitro*, thereby demonstrating its lack of toxicity. However, to selectively evaluate the effects of enhanced astrocyte migration *in vivo*, Ro3303544 administration was restricted to the first 5 days after injury. This protocol allowed us to distinguish the observed results from possible direct axon growth-promoting effects of the drug, because axonal growth is a delayed event.

The observed decrease of astrocyte-devoid spaces filled with CD11b-positive inflammatory cells and the consistent reduction in CSPG- (Fitch & Silver, 1997) and collagen IV-positive areas demonstrated that GSK-3 inhibition at the acute phase of SCI accelerated the compaction of the lesion. We propose that this progressive seclusion of inflammatory cells by reactive astrocytes significantly contributes to the beneficial effect of GSK-3 inhibition after SCI. Although the local inflammatory reaction triggered by SCI is known to be capable of enhancing repair, the involvement of inflammatory cells in secondary neuronal damage such as demyelination is uncontested (Alexander & Popovich, 2009). The beneficial effect of walling off inflammatory cells by scar-forming reactive astrocytes is well established in innate (Bush et al, 1999; Faulkner et al, 2004; Herrmann et al, 2008; Myer et al, 2006; Okada et al, 2006) and adaptive inflammation (Voskuhl et al, 2009).

The major defects observed after ganciclovir-targeted death revealed the contribution of the dividing reactive astrocyte pool to the process of walling off leukocytes after brain and spinal cord injuries (Bush et al, 1999; Faulkner et al, 2004; Myer et al, 2006; Voskuhl et al, 2009). The mitogenic effect of Ro3303544 observed *in vivo* in brain progenitors (Adachi et al, 2007) and *in vitro* in astrocytes led us to investigate whether proliferation was involved in its *in vivo* effect. *In vivo* BrdU incorporation experiments suggest that the contribution of proliferation to the effect of Ro3303544 *in vivo* is not significant.

What is the mechanism whereby the accelerated compaction of inflammatory cells improves functional recovery? Although lesions ultimately demonstrated similar compaction levels at the last time-point examined (42 DPI), locomotor function was permanently superior in the Ro3303544 group compared to control. This observation highlights the critical role of this sub-acute period after the lesion in the recovery process, as previously suggested (Okada et al, 2006). The finding also strongly suggests that white matter sparing is crucial to recovery, as we and others have previously observed when reactive astrocytes wall off inflammatory cells (Faulkner et al, 2004; Herrmann et al, 2008; Okada et al, 2006). Whether remyelination also contributes to the increased myelin staining is difficult to analyse experimentally, as is the conflicting literature concerning the role of β-catenin signalling in remyelination (Azim & Butt, 2011; Fancy et al, 2009).

Given the wide actions of GSK-3 and Wnt/β-catenin, and the role of GSK-3 in inflammation (Jope et al, 2007), additional direct effects of Ro3303544 on inflammatory or immune cells are likely. Nevertheless, the normal infiltration of CD11b cells observed at 7 DPI, the peak of their invasion (Beck et al, 2010), suggests that Ro3303544 does not affect the recruitment of inflammatory cells.

A major question arising from this study is whether our current observation is relevant to other animal models or human SCI. In rat and human, cystic cavity formation is a common complication of brain and spinal cord damage. Unfortunately, these cystic cavities are not observed in most mouse strains, including the C57 BL6/J mice used for this study. *In vitro* studies have suggested that the development of these cavities is closely related to the relationship between inflammatory cells and reactive astrocytes (Fitch et al, 1999). While it is speculated that the physical contraction of the fibrous scar may also contribute to cavity formation in some previous reports (Klapka & Muller, 2006), two recent studies using different experimental approaches have observed that reduction of the scarring was associated with reduced cystic cavities in rat (Iannotti et al, 2006; Xia et al, 2008). However, further studies in relevant models are needed to examine whether the stimulation of reactive astrocyte migration through GSK-3 inhibition does indeed limit the development of these cystic cavities.

In conclusion, our findings reveal a novel beneficial effect of GSK-3 inhibition for SCI and suggest that the pharmacological stimulation of reactive astrocyte migration holds promise as a new therapeutic strategy for the treatment of SCI.

## MATERIALS AND METHODS

### Antibodies and reagents

The antibodies used are listed in Supporting Information. Ro3303544 was developed by Roche and kindly provided by Dr Gary Pelz (Department of Genetics and Genomics, Roche, Palo Alto, California, USA). The initial characterization of Ro3303544 has been reported elsewhere (Adachi et al, 2007). All the experiments reported in

## The paper explained

**PROBLEM:**

**Scarring is a general tissue response after injury to promote wound healing and to separate the injured tissue from the external environment. During the sub-acute phase of contusive SCI, reactive astrocytes migrate to the lesion epicentre and seclude infiltrating inflammatory cells there. This process has been shown to promote functional recovery using several strains of genetically modified mice and models of both innate and adaptive immunity. It is not yet known whether this property of astrocytes can be exploited to aid in the development of better treatment strategies for brain and spinal cord trauma.**

**RESULTS:**

**Taking advantage of a novel, highly potent specific inhibitor of GSK-3, Ro3303544, the authors show that inhibition of GSK-3 stimulates astrocyte migration by regulating the expression of β1-integrin both *in vitro* and *in vivo*. Administration of Ro3303544 for the first 5 days after contusive SCI resulted in faster migration of reactive astrocytes, preservation of more myelinated fibres, and significantly improved recovery of movement. Labelling for CSPG and collagen IV confirmed that Ro3303544 treatment reduced the size of the lesion scar.**

**IMPACT:**

**Here, for the first time, the authors were able to pharmacologically stimulate the beneficial effect of reactive astrocytes on immune cell restriction and scar formation. These findings reveal a novel effect of GSK-3 inhibition that could improve recovery from SCI and suggest that the pharmacological stimulation of reactive astrocyte migration holds promise as a new therapeutic strategy for the treatment of SCI.**

this study compared the effect of Ro3303544 dissolved in DMSO to a control solution that included an equivalent concentration of DMSO (0.1%). BQ-123, BQ-788 and SB415286 were from Sigma.

### Cell culture

See Supporting Information for detailed cell culture methods. Briefly, astrocytes in primary cultures were prepared as previously described (Araujo et al, 1993) from 1-day postnatal wild-type C57BL/6J mice.

### Modified Boyden's chamber assay (transwell assay)

Polyethelene terephthalate (PET) filters with 8-μm pores (BD Biocoat), used to separate the upper and lower chambers, were coated with 10 μg/ml fibronectin (Sigma) or various concentrations of laminin for 3 h at 37°C. Astrocytes were trypsinized on day 13 *in vitro*, stained with trypan blue, and counted using a hemocytometre. A total of $3 \times 10^4$ cells were resuspended in MEM-F12 complete medium containing 1% FBS, 10 μg/ml aphidicolin (Sigma), and the indicated Ro3303544 concentrations, and the cells were allowed to migrate towards the same culture medium supplemented with 10% FBS in the lower chamber. After 15 h at 37°C, the filters were fixed for 20 min at room temperature with 4% paraformaldehyde in PBS (pH 7.5), and the non-migrated cells were removed by wiping the upper side of the membranes with cotton swabs. Cell nuclei were stained using Hoechst 33258, and the filters were mounted on slides in Fluoromount medium (Diagnostic Biosystems). Using Axiovision® software connected to an epifluorescence microscope (Zeiss, Axioplan 2), 12 fields per membrane were captured, and the cells were counted manually.

### SCI model

All surgical and animal-care procedures were in accordance with the Laboratory Animal Welfare Act, the Guide for the Care and Use of Laboratory Animals (National Institutes of Health, USA), and the Guidelines and Policies for Animal Surgery provided by the Animal Study Committee of Murayama Medical Center, and they were approved by the ethics committee of Murayama Medical Center. Adult female C57BL/6J mice (8 weeks of age) were anesthetized with an intraperitoneal injection of ketamine (100 mg/kg) and xylazine (10 mg/kg). The dorsal surface of the dura mater was exposed through a laminectomy at the 10th thoracic vertebra, and SCI was induced using an Infinite Horizon impactor (60 kDyn; Precision Systems & Instrumentation, Lexington KY) as previously described (Scheff et al, 2003). Actual impact forces did not differ between groups (control, $62.83 \pm 2.55$ kDyn; Ro3303544, $62.61 \pm 1.98$ kDyn). The mice were injected intraperitoneally with 0.5 ml Ro3303544 at 500 μM, dissolved in saline or saline containing an equivalent concentration of DMSO (0.1%) twice daily for 5 days, beginning immediately after SCI. The mice were returned to their cages and given free access to water and food.

### Behavioural analysis

Hindlimb motor function was evaluated 1, 3, 7, 14, 21, 28, 35 and 42 days after the injury using the locomotor rating of the BMS (Basso et al, 2006). A team of three experienced examiners evaluated each animal for 4 min and assigned an operationally defined score for each hindlimb, which were then averaged. Animals with incomplete paralysis at 1 DPI (BMS score not equal to zero) were excluded from the study. Data were analysed with two-way repeated measures ANOVA followed by Bonferroni post-hoc test ($n = 12$ and 13 mice in the control and Ro3303544 groups, respectively).

### Immunohistochemistry

Techniques and protocols for immunohistochemistry-based analyses are detailed in Supporting Information.

### Gene microarray analysis

Microarray processing was performed by the Core Instrumentation Facility of Keio University School of Medicine. Detailed procedures are described in Supporting Information. The data set has been deposited

in the NCBI Gene Expression Omnibus (http://www.ncbi.nlm.nih.gov/geo/) and is accessible through GEO series accession number GSE25770.

### Statistical analysis

Data were analysed with one-way ANOVA and Bonferroni's multiple comparison test, unless otherwise specified in the figure legends, using GraphPad Prism software version 5.00 for Windows (GraphPad Software, San Diego, CA, USA).

## Author contributions

FRM conducted all *in vitro* experiments, performed the analysis of lesion volume and demyelination and wrote the paper; HK, TI, AI, AY and SN performed SCI and analysed locomotor function; TI analyzed BrdU incorporation; MMukaino analyzed the lesion scar; KS, MMatsushita and KK provided material; HK, TI, AI, MMukaino, AK, SN, HT, YM, SS and SO analyzed the data and edited the manuscript; YT, MN and HO supervised the study.

## Acknowledgements

We are grateful to Gary Peltz for providing the Ro3303544 and to Shizue Ohsawa for the gift of the HRE-luc constructs. We thank Mari Fujiwara (Core Instrumentation Facility, Keio University School of Medicine) for gene expression microarray processing, Yumi Matsuzaki for advice in flow cytometry, and Tokuko Harada for mouse care. We thank all the members of Dr. Okano's laboratory for helpful discussions and support. This study was supported by the Project for the Realization of Regenerative Medicine and Support for the Core Institutes for iPS Cell Research from the Ministry of Education, Culture, Sports, Science and Technology (MEXT) in Japan, a grant-in-aid for the Global COE Program from MEXT to Keio University, a research grant from Takeda Foundation, by grants-in-aid for scientific research from MEXT (FRM, AI, and MN), fellowships from JST-SORST and the Japan Society for Promotion of Science (JSPS), as well as grants-in-aid from Keio University, JSPS, and the Naito Foundation to FRM.

Supporting information is available at EMBO Molecular Medicine online.

The authors declare that they have no conflict of interest.

## References

Adachi K, Mirzadeh Z, Sakaguchi M, Yamashita T, Nikolcheva T, Gotoh Y, Peltz G, Gong L, Kawase T, Alvarez-Buylla A, *et al* (2007) Beta-catenin signaling promotes proliferation of progenitor cells in the adult mouse subventricular zone. Stem Cells 25: 2827-2836

Akiyama SK, Yamada KM (1987) Biosynthesis and acquisition of biological activity of the fibronectin receptor. J Biol Chem 262: 17536-17542

Alabed YZ, Pool M, Ong Tone S, Sutherland C, Fournier AE (2010) GSK3 beta regulates myelin-dependent axon outgrowth inhibition through CRMP4. J Neurosci 30: 5635-5643

Albiges-Rizo C, Frachet P, Block MR (1995) Down regulation of talin alters cell adhesion and the processing of the alpha 5 beta 1 integrin. J Cell Sci 108: 3317-3329

Alexander JK, Popovich PG (2009) Neuroinflammation in spinal cord injury: therapeutic targets for neuroprotection and regeneration. Prog Brain Res 175: 125-137

Araujo H, Danziger N, Cordier J, Glowinski J, Chneiweiss H (1993) Characterization of PEA-15, a major substrate for protein kinase C in astrocytes. J Biol Chem 268: 5911-5920

Azim K, Butt AM (2011) GSK3beta negatively regulates oligodendrocyte differentiation and myelination in vivo. Glia 59: 540-553

Basso DM, Fisher LC, Anderson AJ, Jakeman LB, McTigue DM, Popovich PG (2006) Basso Mouse Scale for locomotion detects differences in recovery after spinal cord injury in five common mouse strains. J Neurotrauma 23: 635-659

Beck KD, Nguyen HX, Galvan MD, Salazar DL, Woodruff TM, Anderson AJ (2010) Quantitative analysis of cellular inflammation after traumatic spinal cord injury: evidence for a multiphasic inflammatory response in the acute to chronic environment. Brain 133: 433-447

Bush TG, Puvanachandra N, Horner CH, Polito A, Ostenfeld T, Svendsen CN, Mucke L, Johnson MH, Sofroniew MV (1999) Leukocyte infiltration, neuronal degeneration, and neurite outgrowth after ablation of scar-forming, reactive astrocytes in adult transgenic mice. Neuron 23: 297-308

Chico LK, Van Eldik LJ, Watterson DM (2009) Targeting protein kinases in central nervous system disorders. Nat Rev Drug Discov 8: 892-909

Coghlan MP, Culbert AA, Cross DA, Corcoran SL, Yates JW, Pearce NJ, Rausch OL, Murphy GJ, Carter PS, Roxbee Cox L *et al* (2000) Selective small molecule inhibitors of glycogen synthase kinase-3 modulate glycogen metabolism and gene transcription. Chem Biol 7: 793-803

Cuzzocrea S, Genovese T, Mazzon E, Crisafulli C, Di Paola R, Muia C, Collin M, Esposito E, Bramanti P, Thiemermann C (2006) Glycogen synthase kinase-3 beta inhibition reduces secondary damage in experimental spinal cord trauma. J Pharmacol Exp Ther 318: 79-89

Dill J, Wang H, Zhou F, Li S (2008) Inactivation of glycogen synthase kinase 3 promotes axonal growth and recovery in the CNS. J Neurosci 28: 8914-8928

DiMilla PA, Barbee K, Lauffenburger DA (1991) Mathematical model for the effects of adhesion and mechanics on cell migration speed. Biophys J 60: 15-37

Dupin I, Camand E, Etienne-Manneville S (2009) Classical cadherins control nucleus and centrosome position and cell polarity. J Cell Biol 185: 779-786

Etienne-Manneville S, Hall A (2003) Cdc42 regulates GSK-3beta and adenomatous polyposis coli to control cell polarity. Nature 421: 753-756

Fancy SP, Baranzini SE, Zhao C, Yuk DI, Irvine KA, Kaing S, Sanai N, Franklin RJ, Rowitch DH (2009) Dysregulation of the Wnt pathway inhibits timely myelination and remyelination in the mammalian CNS. Genes Dev 23: 1571-1585

Faulkner JR, Herrmann JE, Woo MJ, Tansey KE, Doan NB, Sofroniew MV (2004) Reactive astrocytes protect tissue and preserve function after spinal cord injury. J Neurosci 24: 2143-2155

Fitch MT, Silver J (1997) Activated macrophages and the blood-brain barrier: inflammation after CNS injury leads to increases in putative inhibitory molecules. Exp Neurol 148: 587-603

Fitch MT, Doller C, Combs CK, Landreth GE, Silver J (1999) Cellular and molecular mechanisms of glial scarring and progressive cavitation: in vivo and in vitro analysis of inflammation-induced secondary injury after CNS trauma. J Neurosci 19: 8182-8198

Flugel D, Gorlach A, Michiels C, Kietzmann T (2007) Glycogen synthase kinase 3 phosphorylates hypoxia-inducible factor 1alpha and mediates its destabilization in a VHL-independent manner. Mol Cell Biol 27: 3253-3265

Forde JE, Dale TC (2007) Glycogen synthase kinase 3: a key regulator of cellular fate. Cell Mol Life Sci 64: 1930-1944

Gaudet C, Marganski WA, Kim S, Brown CT, Gunderia V, Dembo M, Wong JY (2003) Influence of type I collagen surface density on fibroblast spreading, motility, and contractility. Biophys J 85: 3329-3335

Herrmann JE, Imura T, Song B, Qi J, Ao Y, Nguyen TK, Korsak RA, Takeda K, Akira S, Sofroniew MV (2008) STAT3 is a critical regulator of astrogliosis and scar formation after spinal cord injury. J Neurosci 28: 7231-7243

Iannotti C, Zhang YP, Shields LB, Han Y, Burke DA, Xu XM, Shields CB (2006) Dural repair reduces connective tissue scar invasion and cystic cavity formation after acute spinal cord laceration injury in adult rats. J Neurotrauma 23: 853-865

Inestrosa NC, Arenas E (2010) Emerging roles of Wnts in the adult nervous system. Nat Rev Neurosci 11: 77-86

Jope RS, Yuskaitis CJ, Beurel E (2007) Glycogen synthase kinase-3 (GSK3): inflammation, diseases, and therapeutics. Neurochem Res 32: 577-595

Kapoor M, Liu S, Shi-wen X, Huh K, McCann M, Denton CP, Woodgett JR, Abraham DJ, Leask A (2008) GSK-3beta in mouse fibroblasts controls wound healing and fibrosis through an endothelin-1-dependent mechanism. J Clin Invest 118: 3279-3290

Klambt C (2009) Modes and regulation of glial migration in vertebrates and invertebrates. Nat Rev Neurosci 10: 769-779

Klapka N, Muller HW (2006) Collagen matrix in spinal cord injury. J Neurotrauma 23: 422-435

Lauffenburger DA, Horwitz AF (1996) Cell migration: a physically integrated molecular process. Cell 84: 359-369

Le QT, Denko NC, Giaccia AJ (2004) Hypoxic gene expression and metastasis. Cancer Metastasis Rev 23: 293-310

Miura K, Okada Y, Aoi T, Okada A, Takahashi K, Okita K, Nakagawa M, Koyanagi M, Tanabe K, Ohnuki M, *et al* (2009) Variation in the safety of induced pluripotent stem cell lines. Nat Biotechnol 27: 743-745

Myer DJ, Gurkoff GG, Lee SM, Hovda DA, Sofroniew MV (2006) Essential protective roles of reactive astrocytes in traumatic brain injury. Brain 129: 2761-2772

Nguyen DX, Chiang AC, Zhang XH, Kim JY, Kris MG, Ladanyi M, Gerald WL, Massague J (2009) WNT/TCF signaling through LEF1 and HOXB9 mediates lung adenocarcinoma metastasis. Cell 138: 51-62

Okada S, Nakamura M, Katoh H, Miyao T, Shimazaki T, Ishii K, Yamane J, Yoshimura A, Iwamoto Y, Toyama Y, *et al* (2006) Conditional ablation of Stat3 or Socs3 discloses a dual role for reactive astrocytes after spinal cord injury. Nat Med 12: 829-834

Okano H (2010) Neural stem cells and strategies for the regeneration of the central nervous system. Proc Jpn Acad Ser B Phys Biol Sci 86: 438-450

Palecek SP, Loftus JC, Ginsberg MH, Lauffenburger DA, Horwitz AF (1997) Integrin-ligand binding properties govern cell migration speed through cell-substratum adhesiveness. Nature 385: 537-540

Renault-Mihara F, Okada S, Shibata S, Nakamura M, Toyama Y, Okano H (2008) Spinal cord injury: emerging beneficial role of reactive astrocytes' migration. Int J Biochem Cell Biol 40: 1649-1653

Salicioni AM, Gaultier A, Brownlee C, Cheezum MK, Gonias SL (2004) Low density lipoprotein receptor-related protein-1 promotes beta1 integrin maturation and transport to the cell surface. J Biol Chem 279: 10005-10012

Scheff SW, Rabchevsky AG, Fugaccia I, Main JA, Lumpp JE Jr., (2003) Experimental modeling of spinal cord injury: characterization of a force-defined injury device. J Neurotrauma 20: 179-193

Sofroniew MV (2009) Molecular dissection of reactive astrogliosis and glial scar formation. Trends Neurosci 32: 638-647

Sun W, Hu W, Xu R, Jin J, Szulc ZM, Zhang G, Galadari SH, Obeid LM, Mao C (2009) Alkaline ceramidase 2 regulates beta1 integrin maturation and cell adhesion. FASEB J 23: 656-666

Takada Y, Ye X, Simon S (2007) The integrins. Genome Biol 8: 215

Tsuji O, Miura K, Okada Y, Fujiyoshi K, Mukaino M, Nagoshi N, Kitamura K, Kumagai G, Nishino M, Tomisato S, *et al* (2010) Therapeutic potential of appropriately evaluated safe-induced pluripotent stem cells for spinal cord injury. Proc Natl Acad Sci USA 107: 12704-12709

van Noort M, Meeldijk J, van der Zee R, Destree O, Clevers H (2002) Wnt signaling controls the phosphorylation status of beta-catenin. J Biol Chem 277: 17901-17905

Voskuhl RR, Peterson RS, Song B, Ao Y, Morales LB, Tiwari-Woodruff S, Sofroniew MV (2009) Reactive astrocytes form scar-like perivascular barriers to leukocytes during adaptive immune inflammation of the CNS. J Neurosci 29: 11511-11522

White RE, Jakeman LB (2008) Don't fence me in: harnessing the beneficial roles of astrocytes for spinal cord repair. Restor Neurol Neurosci 26: 197-214

Xia Y, Zhao T, Li J, Li L, Hu R, Hu S, Feng H, Lin J (2008) Antisense vimentin cDNA combined with chondroitinase ABC reduces glial scar and cystic cavity formation following spinal cord injury in rats. Biochem Biophys Res Commun 377: 562-566

Yoshimura T, Kawano Y, Arimura N, Kawabata S, Kikuchi A, Kaibuchi K (2005) GSK-3beta regulates phosphorylation of CRMP-2 and neuronal polarity. Cell 120: 137-149

STEM CELLS
REGENERATIVE MEDICINE

# Significance of Remyelination by Neural Stem/Progenitor Cells Transplanted into the Injured Spinal Cord

AKIMASA YASUDA,[a,b] OSAHIKO TSUJI,[a] SHINSUKE SHIBATA,[b] SATOSHI NORI,[a,b] MORITO TAKANO,[a,b] YOSHIOMI KOBAYASHI,[a,b] YUICHIRO TAKAHASHI,[a,b] KANEHIRO FUJIYOSHI,[a] CHIKAKO MIYAUCHI HARA,[b,c] ATSUHI MIYAWAKI,[c] HIROTAKA JAMES OKANO,[b] YOSHIAKI TOYAMA,[a] MASAYA NAKAMURA,[a] HIDEYUKI OKANO[b,d]

[a]Department of Orthopedic Surgery and [b]Department of Physiology, Keio University School of Medicine, Tokyo, Japan; [c]Laboratory for Cell Function and Dynamics, Advanced Technology Development Group and [d]RIKEN-Keio University Joint Research Laboratory, Brain Science Institute, RIKEN, Saitama, Japan

**Key Words.** Spinal cord injury • Neural stem cell • Stem-cell transplantation • Oligodendrocytes • Remyelination • *shiverer* mutant mouse

ABSTRACT

**Previous reports of functional recovery from spinal cord injury (SCI) in rodents and monkeys after the delayed transplantation of neural stem/progenitor cells (NS/PCs) have raised hopes that stem cell therapy could be used to treat SCI in humans. More research is needed, however, to understand the mechanism of functional recovery. Oligodendrocytes derived from grafted NS/PCs remyelinate spared axons in the injured spinal cord. Here, we studied the extent of this remyelination's contribution to functional recovery following contusive SCI in mice. To isolate the effect of remyelination from other possible regenerative benefits of the grafted cells, NS/PCs obtained from myelin-deficient *shiverer* mutant mice (*shi*-NS/PCs) were used in this work alongside wild-type NS/PCs (*wt*-NS/PCs). *shi*-NS/PCs behaved like *wt*-NS/PCs in vitro and in vivo, with the exception of their myelinating potential. *shi*-NS/PC-derived oligodendrocytes did not express myelin basic protein in vitro and formed much thinner myelin sheaths in vivo compared with *wt*-NS/PC-derived oligodendrocytes. The transplantation of *shi*-NS/PCs promoted some locomotor and electrophysiological functional recovery but significantly less than that afforded by *wt*-NS/PCs. These findings establish the biological importance of remyelination by graft-derived cells for functional recovery after the transplantation of NS/PCs into the injured spinal cord.** STEM CELLS *2011;29:1983–1994*

Disclosure of potential conflicts of interest is found at the end of this article.

## INTRODUCTION

Traumatic spinal cord injury (SCI) results in severe and permanent neurological deficits that can include paraplegia and tetraplegia. However, there is currently no effective clinical therapeutic option to improve the functional outcome following SCI. Recent advances in stem cell biology are clearing the way toward implementing therapeutic strategies to replace lost neural cells through the transplantation of stem cells. Such strategies could be applicable to many central nervous system (CNS) disorders, and SCI may be one of the first conditions treated with stem-cell transplantation therapy. To this point, embryonic stem cells (ESCs), bone marrow mesenchymal stem cells, and glial-restricted precursor cells have all been reported to induce functional improvement following their transplantation into the injured spinal cord [1–6].

In particular, we and others have reported beneficial effects and improved functional recovery in experimental SCI models following the transplantation of neural stem/progenitor cells (NS/PCs) derived from the CNS [3, 6-10] or from pluripotent stem cells, including ESCs [11–14] and induced pluripotent stem cells (iPSCs) [15, 16]. Notably, Cummings and colleagues showed that selective ablation of grafted cells resulted in the subsequent deterioration of motor function in animals that had initially demonstrated functional motor recovery after SCI. This indicates that the long-term survival of grafted cells in the host spinal cord is very important for the maintenance of functional recovery [3].

Although the underlying mechanism responsible for functional recovery from SCI after stem-cell transplantation has still remained unclear [17, 18], three mechanisms have been proposed: the replacement of lost neurons to reconstruct local circuitry, the remyelination of spared, demyelinated axons by

Author contributions: A.Y.: conception and design, experiments, data analysis and interpretation, manuscript writing, and final approval of manuscript; O.T.: conception and design, experiments, surgery, and data analysis and interpretation, S.S.: experiments and data analysis and interpretation, S.N.: experiments, surgery, and data interpretation; M.T.: experiments, surgery, and data analysis; Y.K. and Y.T.: experiments and data interpretation; K.F., C.M.H., A.M., H.J.O. and Y.T.: data analysis and interpretation; M.N. and H.O.: conception and design, data analysis and interpretation, manuscript writing, and final approval of manuscript.

Correspondence: Hideyuki Okano, M.D., Ph.D., Department of Physiology, School of Medicine, Keio University, 35 Shinanomachi, Shinjuku, Tokyo 160-8582, Japan. Telephone: +81-3-5363-3747; Fax: +81-3-3357-5445; e-mail: hidokano@a2.keio.jp; or Masaya Nakamura, M.D., Ph.D., Department of Orthopedic surgery, School of Medicine, Keio University, 35 Shinanomachi, Shinjuku, Tokyo 160-8582, Japan. Telephone: +81-3-3353-1211; Fax: +81-3353-6597; e-mail: masa@sc.itc.keio.ac.jp, masa@a8.keio.jp Received June 6, 2011; accepted for publication October 5, 2011; first published online in STEM CELLS *EXPRESS* October 25, 2011. © AlphaMed Press
1066-5099/2011/$30.00/0 doi: 10.1002/stem.767

graft-derived oligodendrocytes, and the provision of trophic support that reduces the damage and creates a permissive substrate for axonal growth. In previous studies, the transplantation of NS/PCs derived from various sources into mouse SCI models [3, 6, 12, 15] resulted in the remyelination of spared axons by graft-derived oligodendrocytes and good recovery of locomotor function after SCI. These findings could imply that graft-derived oligodendrocytes play a role in functional recovery. However, a causative relationship between the actions of graft-derived oligodendrocytes, including remyelination, and the observed functional recovery has not been fully addressed.

In this study, we analyzed the importance of graft-derived oligodendrocytes to functional recovery after SCI by comparing the transplantation of NS/PCs from wild-type mice with NS/PCs from myelin-deficient *shiverer* mutant mice [19–21]. The latter have a partial deletion in the gene encoding myelin basic protein (MBP) [22–25]. The present data establish the importance of graft-derived oligodendrocytes in the functional recovery of the injured spinal cord after NS/PC transplantation. This insight will be crucial for extending stem-cell-based therapy to SCI repair.

## Materials and Methods

### NS/PC Cultures

The methods for culture and expansion of NS/PCs were as described previously [26]. In brief, the striata of Jcl:ICR (ICR) background homozygous *shiverer* mutant mice and wild-type C57BL/6J mice on embryonic day 14 were dissociated using a fire-polished glass pipette. The dissociated cells were collected by centrifugation and resuspended in culture medium followed by cell cluster (neurosphere) formation. For differentiation, the neurospheres were cultured without serum or growth factors. In vitro myelin marker assay was performed with the method modified from Stankoff et al. [27] (See Supporting Information Materials and Methods).

The proliferation assay was performed by measuring ATP, which indirectly reflects the number of viable cells. Population doubling times were determined using the ATP assay, as described elsewhere [28, 29]. Trophic factor analysis was also performed, as described previously [30] (See Supporting Information).

### Animal Model

Adult female NOD/SCID (NOD.CB17-Prkdcscid/J) mice (8–10 week old, 20–22 g, $n = 42$; Charles River Laboratories, Kanagawa, Japan) were anesthetized with an intraperitoneal (i.p.) injection of ketamine (100 mg/kg) and xylazine (10 mg/kg). After laminectomy at the 10th thoracic spinal vertebra ($T_{10}$), the dorsal surface of the dura mater was exposed. SCI was induced as described previously [31], using a commercially available SCI device (IH impactor, Precision Systems and Instrumentation, Lexington, KY, USA; http://www.presysin.com). This device creates a reliable contusion injury by rapidly applying a force-defined impact (60 kdyn) with a stainless steel-tipped impactor. All experiments were performed in accordance with the Guidelines for the Care and Use of Laboratory Animals of Keio University School of Medicine and the Guide for the Care and Use of Laboratory Animals (National Institutes of Health, Bethesda, MD, USA).

### Cell Transplantation

A fusion HIV-1 based lentiviral vector, expressing ffLuc (Venus fused to firefly luciferase) under the control of the elongation factor 1α (EF1α) promoter [30], was used to label NS/PCs prior to grafting. This vector enabled the detection of grafted cells as strong bioluminescent ffLuc signals in live SCI mice and as fluorescent Venus signals using anti-green fluorescent protein antibody in fixed spinal-cord sections. This virus was obtained as previously reported [32]. The concentrated virus was added to the culture medium to infect primary NS/PCs derived from *shiverer* or wild-type mice (multiplicity of injection = 1.0). The lentivirally transduced NS/PCs ($5 \times 10^5$ cells per two microliters) were transplanted into the lesion epicenter 9 days after SCI as previously reported [11, 12, 15, 16, 31-33].

The NS/PCs were injected with a glass micropipette at a rate of 1 μl/minute with a Hamilton syringe (25 μl) and a stereotaxic microinjector (KDS 310, Muromachikikai Co. Ltd., Tokyo, Japan, http://www.muromachi.com). *shi*-NS/PCs were transplanted into 15 mice (*shi*-NS/PC group), and *wt*-NS/PCs were transplanted into 13 mice (*wt*-NS/PC group). Phosphate-buffered saline (PBS; 2 μl per mouse) was injected into the lesion epicenter of control mice (control group; $n = 14$). After surgery, animal care was performed in the Supporting Information.

### Bioimaging

The Xenogen-IVIS spectrum cooled charge-coupled device (CCD) optical macroscopic imaging system (Caliper Life-Sciences, Hopkinton, MA, USA; http://www.caliperls.com) was used for bioimaging to confirm the survival of the transplanted NS/PCs. Monitoring was performed for 6 weeks after the transplantation, as described previously with slight modification [31] (See Supporting Information).

### Motor Function Analysis

Hind limb motor function was evaluated for 7 weeks after SCI using the locomotor rating test of the Basso Mouse Scale (BMS) [34]. Well-trained investigators, blinded to the treatments, performed the behavioral analysis, determining the BMS scores at the same time each day. We also measured the motor function of each group ($n = 5$ each) on a rotating rod apparatus (Muromachikikai Co., Ltd., Japan), consisting of a plastic rod (3-cm diameter, 8-cm long) with a gritted surface, flanked by two large discs (40-cm diameter). At 7 weeks after SCI, mice from each group were tested by monitoring the time that each mouse spent on the rod as it rotated at 10 rpm during 2-minute sessions [35]. Three trials were conducted, and the average and maximum numbers of seconds were recorded. Gait analysis was performed using the DigiGait Image Analysis System (Mouse Specifics, Quincy, MA, USA; http://www.mousespecifics.com). Data collection for DigiGait analysis was performed 7 weeks after injury, when each mouse demonstrated consistent weight-supported hind limb stepping on the treadmill at a speed of 8 cm/sec.

### Histological Analyses

Animals were anesthetized and transcardially perfused with 4% paraformaldehyde in 0.1 M PBS, 6 weeks after transplantation. The spinal cords were removed, embedded in Optimal Cutting Temperature compound (Sakura Finetechnical Co., Ltd., Tokyo, Japan; http://www.sakuraus.com), and sectioned in the sagittal/axial plane at 12 μm on a cryostat (Leica CM3050 S, Leica Microsystems, Wetzlar, Germany; http://www.leica.com). Sections were stained with hematoxylin-eosin (HE), or Luxol Fast Blue (LFB), or processed for immunohistochemistry followed by quantitative analyses. Samples were examined on an inverted fluorescence microscope (BZ 9000; Keyence Co., Osaka, Japan; http://www.keyence.co.jp) or a confocal laser-scanning microscope (LSM 700, Carl Zeiss, Munchi, Germany; http://www.zeiss.

com). We also performed immuno-electron microscopic analyses (See Supporting Information).

### Electrophysiology

Electrophysiological experiments were performed immediately after injury, immediately after transplantation, and 7 weeks after injury. An electromyography (EMG)/evoked potential measuring system (Neuropack S1 MEB-9400 series, Nihon Kohden, Tokyo, Japan; http://www.nihonkohden.co.jp) was used. Mice were anesthetized with an i.p. injection of ketamine (40 mg/kg) and xylazine (4 mg/kg), as described in other paper [16]. One electrode was injected into the spinal cord of the occipito-cervical area to induce motor-evoked potential (MEP) and the sciatic nerve to induce compound motor action potential (CMAP). For the recording of the potentials, two needle electrodes were placed in each hind limb. The active electrode was placed in the muscle belly of each limb, and the reference electrode was placed near the distal tendon of the muscle. The ground electrode was placed subcutaneously between the coil and the recording electrodes. To induce MEP, a stimulation of 0.4 mA intensity was applied at the electrode [16].

Throughout the experiments, the duration of the pulse was 0.2 ms. CMAPs were recorded by measuring the maximum amplitude that was achieved by stimulating the sciatic nerve with a single pulse of supramaximal intensity. The onset latency was measured as the length of time in milliseconds between the stimulus and the onset of the first wave. The amplitude (mV) was measured from the initiation point of the first wave to its highest point. Results were expressed as the MEP/CMAP ratio (%) so as to adjust for differences between individual mice [14, 36]. Ten responses were averaged and sorted for off-line analysis.

### Statistical Analyses

All data are presented as the mean ± SEM. An unpaired two-tailed Student's *t* test was used for determining significant differences between groups in the in vitro and in vivo differentiation assays, the bioimaging analysis, analyses of the Venus-positive areas, and MEP analyses. Analysis of variance (ANOVA) followed by the Tukey-Kramer test for multiple comparisons among the three transplantation groups was used for the 5-hydroxytryptamine(HT) analysis, Rota-rod and gait analysis. Repeated measures two-way ANOVA followed by the Tukey-Kramer test was used for analysis of the HE-, LFB-, and neurofilament-heavy chain (NF-H)-stained sections and BMS scores. For all statistical analyses, the significance was set at $p < .05$.

## Results

### In Vitro Characterization of NS/PCs Derived from *shiverer* Mutant Mice Embryos

For the in vitro characterization of NS/PCs derived from *shiverer* mutant mice, proliferation and differentiation assays were performed. *shi*-NS/PCs and *wt*-NS/PCs were cultured as neurospheres, as previously reported [26, 37]. The *shi*-NS/PCs formed floating cell clusters (neurospheres) within 2–3 days (Supporting Information Fig. 1A), with a morphology identical to that of the *wt*-NS/PC-derived neurospheres (Supporting Information Fig. 1B). The proliferation rates of the *shi*-NS/PCs and *wt*-NS/PCs were evaluated indirectly by measuring the production of ATP. There was no significant difference in the doubling time between *shi*-NS/PCs and *wt*-NS/PCs (26.7 ± 1.3 hours vs. 26.1 ± 1.3 hours) (Supporting Information Fig. 1C).

An in vitro differentiation assay revealed that both *shi*-NS/PCs and *wt*-NS/PCs differentiated into neuron-specific class III beta tubulin (Tuj-1)$^+$ neurons, glial fibrillary acidic protein (GFAP)$^+$ astrocytes, and 2′3′-cyclic nucleotide 3′-phosphodiesterase (CNPase)$^+$ oligodendrocytes (Fig. 1A). There were no significant differences in the proportions of the different cell types generated between the *shi*-NS/PCs and *wt*-NS/PCs (Tuj-1, 7.7 ± 1.1% vs. 8.1 ± 0.8%; GFAP, 65.4 ± 1.9% vs. 64.9 ± 1.8%; CNPase, 9.2 ± 1.3% vs. 8.7 ± 0.6%; Fig. 1B). Next, oligodendroglial differentiation was examined via the addition of platelet-derived growth factor (PDGF)-AA and ciliary neurotrophic factor (CNTF) to promote in vitro myelination [27]. Although the *wt*-NS/PCs produced O1$^+$, CNPase$^+$, proteolipid protein (PLP)$^+$, and MBP$^+$ oligodendrocytes, the *shi*-NS/PCs produced oligodendrocytes positive for O1, CNPase, and PLP but negative for MBP (Fig. 1C, 1D).

### Grafted *shi*-NS/PCs and *wt*-NS/PCs Survived Within the Injured Spinal Cord

To identify and monitor the transplanted cells in the injured spinal cord, both *shi*-NS/PCs and *wt*-NS/PCs were transduced to express ffLuc under the EF1α promoter by lentiviral infection. Because of the stable and strong emission of ffLuc, which is a fusion protein of Venus and luciferase, we could identify the grafted cells as fluorescent Venus signals and bioluminescent luciferase signals (C.M. Hara et al., manuscript submitted for publication). Prior to the transplantation, we confirmed that ffLuc was expressed in the *shi*-NS/PCs by fluorescence microscopy (Fig. 2A) and was detectable by the IVIS bioimaging system. We also confirmed the ffLuc transduction into *wt*-NS/PCs, as previously reported [32]. Next, *shi*-NS/PCs or *wt*-NS/PCs were transplanted into the lesion site of NOD/SCID mice 9 days after contusive SCI.

The successful transplantation of *shi*-NS/PCs and *wt*-NS/PCs could be confirmed immediately by bioluminescence imaging (BLI); the average signal intensity was (1.7 ± 0.5) × $10^8$ photons per mouse per sec in the transplanted mice. The BLI analysis revealed that the signal intensity of the grafted cells decreased sharply within the first week after transplantation but remained at approximately 20% of the initial signal intensity in both *shi*-NS/PCs and *wt*-NS/PC groups throughout the remaining period (Fig. 2C). After 6 weeks of transplantation, the survival of both grafted *shi*-NS/PCs and *wt*-NS/PCs in and around the lesion site was detected in tissue sections by anti-Venus immunostaining (Fig. 2D). There was no significant difference in the survival rate detected by BLI between the *shi*-NS/PCs and *wt*-NS/PCs groups (21.5 ± 1.5% vs. 18.3 ± 1.4%), which was also confirmed by quantitative histological analysis of the Venus$^+$ area (0.021 ± 0.003 mm$^2$ vs. 0.024 ± 0.004 mm$^2$) 6 weeks after transplantation (Fig. 2E). Next, the migration of grafted cells was analyzed by comparing Venus$^+$ areas in axial sections of the spinal cord for each group. No significant migratory differences were revealed in and around the lesion site (Fig. 2F, 2G).

### Grafted *shi*-NS/PCs and *wt*-NS/PCs Exhibited Similar Differentiation Potential

To examine the differentiation potential of *shi*-NS/PCs grafted into the injured spinal cord, we performed immunohistochemical analyses 6 weeks after transplantation. The *shi*-NS/PCs differentiated into Hu$^+$ neurons, GFAP$^+$ astrocytes, and APC$^+$ oligodendrocytes (Fig. 3A). A comparison between the cell types that differentiated from the *shi*-NS/PCs and *wt*-NS/PCs in vivo showed no significant differences (Hu$^+$, 9.1 ± 0.5% vs. 9.2 ± 1.0%; GFAP$^+$, 54.3 ± 2.0% vs. 56.7 ±

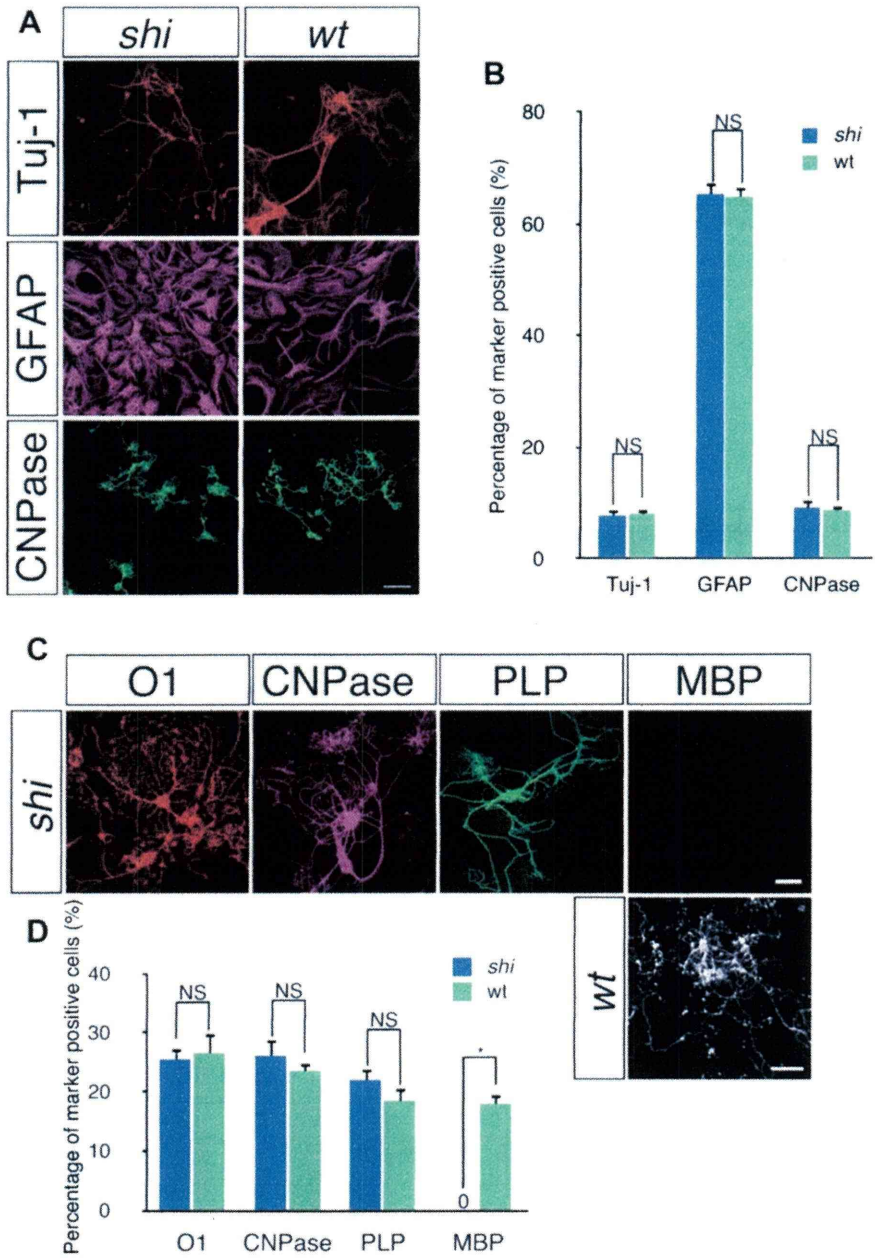


**Figure 1.** In vitro differentiation characteristics of *shi*-neural stem/progenitor cells (NS/PCs). **(A):** *shi*-NS/PCs differentiated into Tuj-1$^+$ neurons, GFAP$^+$ astrocytes, and CNPase$^+$ oligodendrocytes, like *wt*-NS/PCs. Scale bar = 50 μm. **(B):** There were no significant differences in the proportion of differentiated cells generated by the *shi*-NS/PCs versus the *wt*-NS/PCs. **(C):** After adding platelet-derived growth factor AA and ciliary neurotrophic factor to the culture medium, both *wt*-NS/PCs and *shi*-NS/PCs differentiated into O1$^+$, CNPase$^+$, and PLP$^+$ oligodendrocytes. Oligodendrocytes from *shi*-NS/PCs showed no MBP expression, as expected [22–24]. Scale bar = 20 μm. **(D):** O1, CNPase, and PLP immunostaining assays showed no significant difference between the *shi*-NS/PCs and *wt*-NS/PCs, but MBP$^+$ oligodendrocytes were only seen in cultures of *wt*-NS/PCs (*$p$, < .01). Abbreviations: CNPase, 2′3′-cyclic nucleotide 3′-phosphodiesterase; GFAP, glial fibrillary acidic protein; MBP, myelin basic protein; PLP, proteolipid protein; *shi*, *shiverer*; Tuj1, neuron-specific class III beta tubulin; wt, wild type.

2.4%; APC$^+$, 33.7 ± 1.7% vs. 30.0 ± 2.2% [Fig. 3B]), similar to our findings in vitro. Thus, the *shi*-NS/PCs and *wt*-NS/PCs gave rise to similar differentiated cell types in vivo as well as in vitro.

## Transplanted *shi*-NS/PCs Prevented Atrophic Changes in the Injured Spinal Cord and Promoted Axonal Growth After SCI

To examine the effects of *shi*-NS/PC transplantation on the injured spinal cord, we first evaluated the amount of atrophy, by HE staining (Fig. 4A). The transverse area of the spinal cord at the lesion epicenter was significantly larger in both the *shi*-NS/PC and *wt*-NS/PC groups than in the control group, and there was no difference between the amount of enlargement in the experimental groups, suggesting that *shi*-NS/PCs and *wt*-NS/PCs provided equivalent protection from atrophy (Fig. 4B). Next, we examined the effects of transplanted *shi*-NS/PCs on axonal growth after SCI by immunohistochemical analyses, with anti-NF-H (RT97) and anti-5-hydroxytryptamine (5-HT) antibodies. Although a few NF-H$^+$ axons were observed at the rim of the epicenter in the control

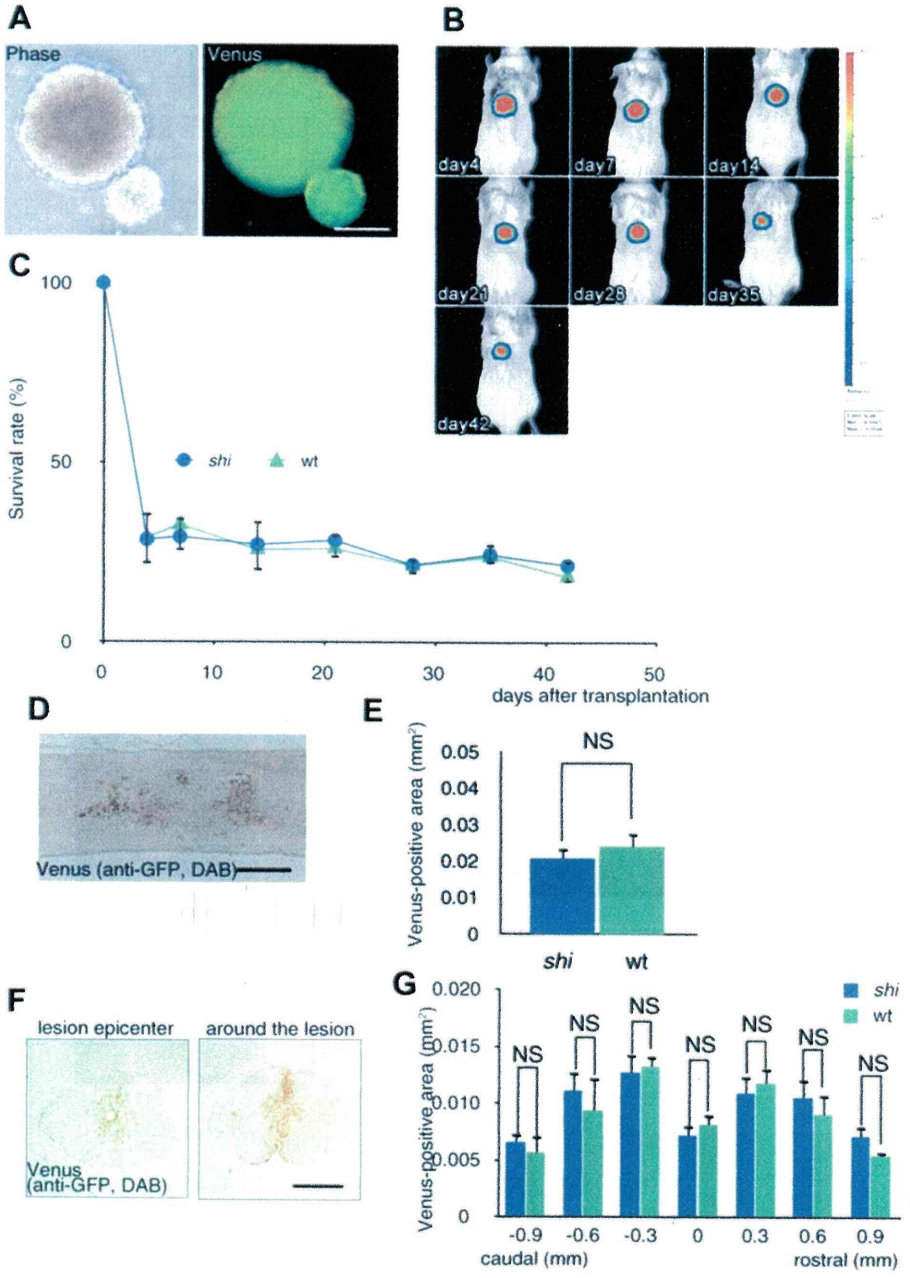


**Figure 2.** Survival of grafted *shi*-neural stem/progenitor cells (NS/PCs) in the injured spinal cord. **(A):** Fluorescence and phase-contrast images of *shi*-NS/PCs-derived neurospheres just before transplantation. Scale bar = 100 μm. **(B):** Representative in vivo images of *shi*-NS/PCs transplanted into the injured spinal cord of an adult NOD/SCID mouse. Survival of grafted *shi*-NS/PCs was detected for 42 days after the transplantation. **(C):** Quantitative analysis of photon counts in recipients of *shi*-NS/PC and *wt*-NS/PC grafts revealed no significant difference in the survival rate of the grafted cells for 42 days after the transplantation ($n = 6$ mice per group, two-tailed $t$ test). **(D):** Representative image of a midsagittal section of a *shi*-NS/PC-grafted spinal cord that was immunostained for Venus using an anti-GFP antibody. Scale bar = 500 μm. **(E):** Quantitative analysis of the Venus-positive area at the lesion epicenter revealed no significant difference between the *shi*-NS/PC and *wt*-NS/PC groups 6 weeks after transplantation ($n = 4$). **(F):** Representative images of an axial section of lesion epicenter (left) and the area surrounding the lesion (0.6-mm rostral from the lesion site: right) immunostained for Venus using an anti-GFP antibody. **(G):** Quantitative analysis of the migration of grafted cells as assessed on the Venus-immunostained sections revealed no significant differences between *shi*-NS/PC and *wt*-NS/PC groups at and around the lesion site ($n = 4$ mice per group). Abbreviations: DAB, diaminobenzidine; GFP, green fluorescent protein; NOD/SCID, NOD/SCID (NOD.CB17-Prkdcscid/J); *shi*, *shiverer*; wt, wild type.

PBS-injected group (Fig. 4C), there were significantly more NF-H$^+$ neuronal fibers in the *shi*-NS/PC and *wt*-NS/PC groups, at the lesion epicenter and at sites rostral and caudal to it (Fig. 4D); the same effect was seen for 5-HT$^+$ serotonergic fibers at the lumbar enlargement, which are critical for hind limb locomotor functions [38–40] (Fig. 4E, 4F).

## Grafted *wt*-NS/PCs, but not *shi*-NS/PCs, Preserved and/or Enhanced Myelination Within the Injured Spinal Cord

In the control group, contusive SCI resulted in severe demyelination at the lesion site. Both the grafted *shi*-NS/PCs and *wt*-NS/PCs showed preserved and/or enhanced myelination

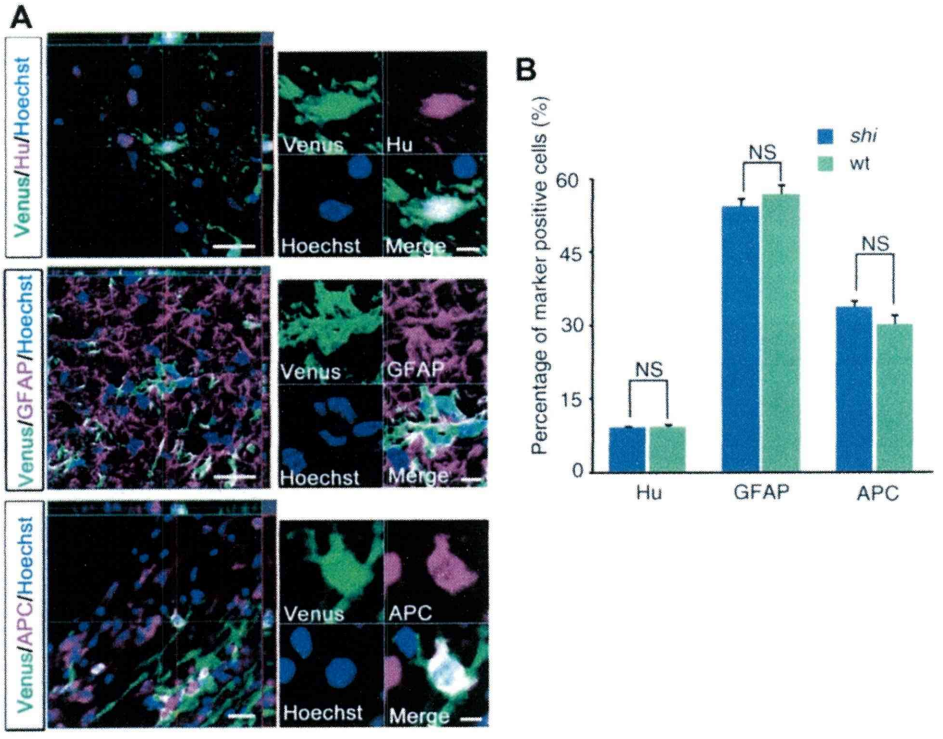


**Figure 3.** In vivo differentiation characteristics of *shi*-neural stem/progenitor cells (NS/PCs) grafted into the injured spinal cord of NOD/SCID mice. **(A):** *shi*-NS/PCs differentiated into $Hu^+$ neurons, $GFAP^+$ astrocytes, and $APC^+$ oligodendrocytes in vivo as well as in vitro. Scale bar = 20 $\mu$m (left), 5 $\mu$m (right). **(B):** The pattern of the differentiated phenotypes was also identical between the *shi*-NS/PCs and *wt*-NS/PCs in vivo ($n$ = 5 mice per group). Abbreviations: APC, adenomatous polyposis coli antigen (APC: clone. CC1); GFAP, glial fibrillary acidic protein; Hu; NOD/SCID, NOD/SCID (NOD.CB17-Prkdcscid/J); *shi*, *shiverer*; wt, wild type.

after SCI, compared with controls. Notably, the *wt*-NS/PC group showed the largest $LFB^+$ myelination area among the three groups (Fig. 5A, 5B, 5C). Consistent with this finding, $Venus^+/MBP^+$ double-labeled myelin sheaths were seen in the *wt*-NS/PC group but none were observed in the *shi*-NS/PC group (Fig. 5D, 5E, 5F). We confirmed these findings by immuno-electron microscopy (EM). In the *shi*-NS/PC group, there were a few axonal profiles showing poor myelination with $Venus^+$ labeling, whereas in the *wt*-NS/PC group, profiles showing mature, $Venus^+$ myelin sheaths were present. Immuno-EM examination under higher magnification revealed nanogold-labeled $Venus^+$ spots in the outer and inner mesaxons of the myelin cytoplasm (Fig. 5G, 5H). These findings suggest that *shi*-NS/PC-derived oligodendrocytes made only thin, poorly formed myelin sheathes, but those derived from *wt*-NS/PCs were capable of forming mature sheathes on remyelinated axons.

## Transplanted *wt*-NS/PCs, but Not *shi*-NS/PCs, Enhanced Significant Locomotor Functional Recovery After SCI

We assessed locomotor functional recovery using the BMS scoring of open field walking, the rota-rod treadmill test, and gait analysis. We used PBS-injected animals as a negative control, which exhibit little difference in BMS scores compared to another negative control animals with fibroblast transplantation [15].

Just after SCI (day 1), the animals exhibited complete hind limb paralysis (BMS score 0), followed by gradual recovery that plateaued at around 4 weeks, in the control group. Although there was no significant difference in the BMS scores among the control, *shi*-NS/PC, and *wt*-NS/PC groups at 2 weeks after SCI, mice of the *wt*-NS/PC group had significantly higher BMS scores than the control group mice on day 28 and thereafter. Conversely, the *shi*-NS/PC group showed a little functional recovery soon after transplantation but it was not statistically significant. By 6 weeks after transplantation, the BMS score of the *wt*-NS/PC group was significantly higher than that of the *shi*-NS/PC group (3.9 $\pm$ 0.2 vs. 3.0 $\pm$ 0.1; Fig. 6A). These data were consistent with the results of the rota-rod treadmill and gait analyses. In the rota-rod treadmill test, the *wt*-NS/PC-transplanted mice remained on the rod significantly longer than those of the control group, whereas the *shi*-NS/PC-transplanted mice fell off the rod with the similar timing to the control group (Fig. 6B). Gait characteristics were measured with the DigiGait Image Analysis System. Stride length was significantly greater in the *wt*-NS/PC group than in the control group; however, the *shi*-NS/PC group showed no significant difference compared with controls (Fig. 6C).

Finally, an MEP analysis was performed as an electrophysiological assessment to measure the MEP latency and amplitude and to examine signal conduction in the injured spinal cord. The latency of the MEP was measured from the onset of the stimulus to the first response to each wave. None of the mice demonstrated an MEP response immediately after SCI or immediately after NS/PC transplantation (9 days after SCI; Supporting Information Fig. 2). At 6 weeks after *shi*-NS/PC transplantation, we detected MEP response of which latency was significantly longer than that obtained after *wt*-NS/PC transplantation (15.7 $\pm$ 0.7 ms vs. 8.0 $\pm$ 0.7 ms). Furthermore, MEP amplitude of *shi*-NS/PC group was significantly smaller than that of *wt*-NS/PC group (MEP/CMAP 0.5 $\pm$ 0.1% vs. 0.8 $\pm$ 0.1%; Fig. 6F). By contrast, no MEP response was detected in the control group under our experimental

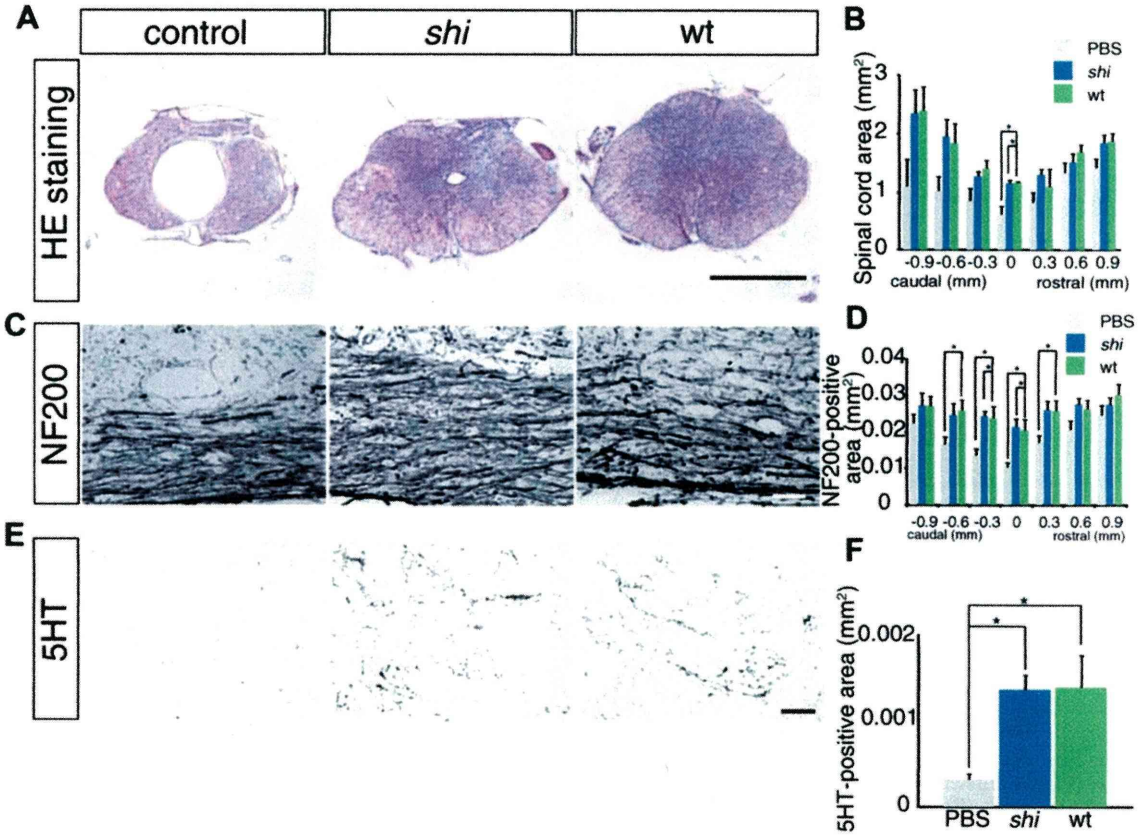


**Figure 4.** Effects of transplanted *shi*-neural stem/progenitor cells (NS/PCs) in the injured spinal cord. **(A):** Representative HE staining images of an axially sectioned spinal cord at the lesion epicenter, 7 weeks after injury. **(B):** Quantitative analysis of the spinal cord area measured in HE-stained axial sections through different regions. The transverse area of the spinal cord at the lesion epicenter was significantly larger in the *shi*-NS/PC and *wt*-NS/PC groups than the vehicle control group ($n = 4$ mice per group). **(C):** Representative images of sagittal sections stained for NF-H, from in all three groups, showing the rim of the lesion epicenter. **(D):** Quantitative analysis of the NF-H$^+$ area at each distance point. While few NF-H$^+$ neuronal fibers were seen at the lesion epicenter in the control group, there were significantly more NF-H$^+$ neuronal fibers in the *shi*-NS/PC and *wt*-NS/PC groups. This was also true at 0.3-mm caudal to the lesion. At 0.6-mm caudal and 0.3-mm rostral to the lesion, the *wt*-NS/PC group had significantly more NF-H$^+$ fibers than the control group ($n = 4$). **(E):** Representative images from all three groups of axial sections stained for 5-HT at the lumbar enlargement. **(F):** Quantitative analysis of the 5-HT$^+$ area in axial sections at the lumbar enlargement. Significantly more 5-HT$^+$ fibers were observed in the *shi*-NS/PC and *wt*-NS/PC group than in the control group ($n = 4$; *: $p, < .05$ in (B), (D), and (F)). Scale bars = 500 $\mu$m in (A), 50 $\mu$m in (C) and (E). Abbreviations: HE, hematoxylin-eosin; 5-HT, 5-hydroxytryptamine; NF, neurofilament; PBS, phosphate-buffered saline; *shi*, *shiverer*; wt, wild type.

conditions (Fig. 6D). These data support a critical role for signal conduction in the extent of hind limb locomotor functional recovery following NS/PC transplantation.

## Discussion

There is increasing interest in stem-cell transplantation for the diseased or injured CNS, including for SCI. Considering their clinical application, the precise mechanisms of action of many stem-cell populations still remain to be elucidated at the preclinical level. Theoretically, possible mechanisms of therapeutic effects of stem-cell transplantation in CNS diseases/injuries include: (a) cell replacement for lost cells after CNS damage (e.g., forming new oligodendrocytes and/or neurons) and (b) trophic support to increase survival of host neural cells and host-mediated regeneration, repair, and/or plasticity [3, 41]. While the latter mechanisms include short-term neurotrophic/neuroprotective effects, the graft-derived cells should differentiate into the appropriate cells and survive over the long-term to achieve functional recovery through the cell replacement.

Accordingly, to obtain long-term survival of graft-derived cells in the damaged host CNS and to investigate the role of graft-mediated remyelination in this study, we used a constitutively immunodeficient animal model, NOD/SCID mice, as hosts. NOD/SCID mice lack normal T-cell, B-cell, and complement responses [42, 43]. The use of NOD/SCID mice is known to result in a greater cell survival and engraftment for allograft and xenograft in comparison with conventional immunosuppressant treatment, that is, cyclosporin A or FK506, which targets T-cell activation/proliferation via disrupting calcineurin signaling. In most models using with conventional pharmacologic immunosuppression, there is a progressive loss of cells for more than 1–4 months. In the initial experiments for this study, we performed allografts using different mouse strains as grafts and recipients to investigate the effects of NS/PCs derived from myelin-deficient *shiverer* mutant versus wild-type mice. We maintain *shiverer* mutant mice with the ICR background as a homozygous closed colony. Because mice with the ICR background have been poorly characterized with respect to histopathology or behavioral assays after SCI, we selected C57BL/6J mice as the host for NS/PC transplants. However, when *shi*-NS/PCs with the ICR background were transplanted into C57BL/6J hosts

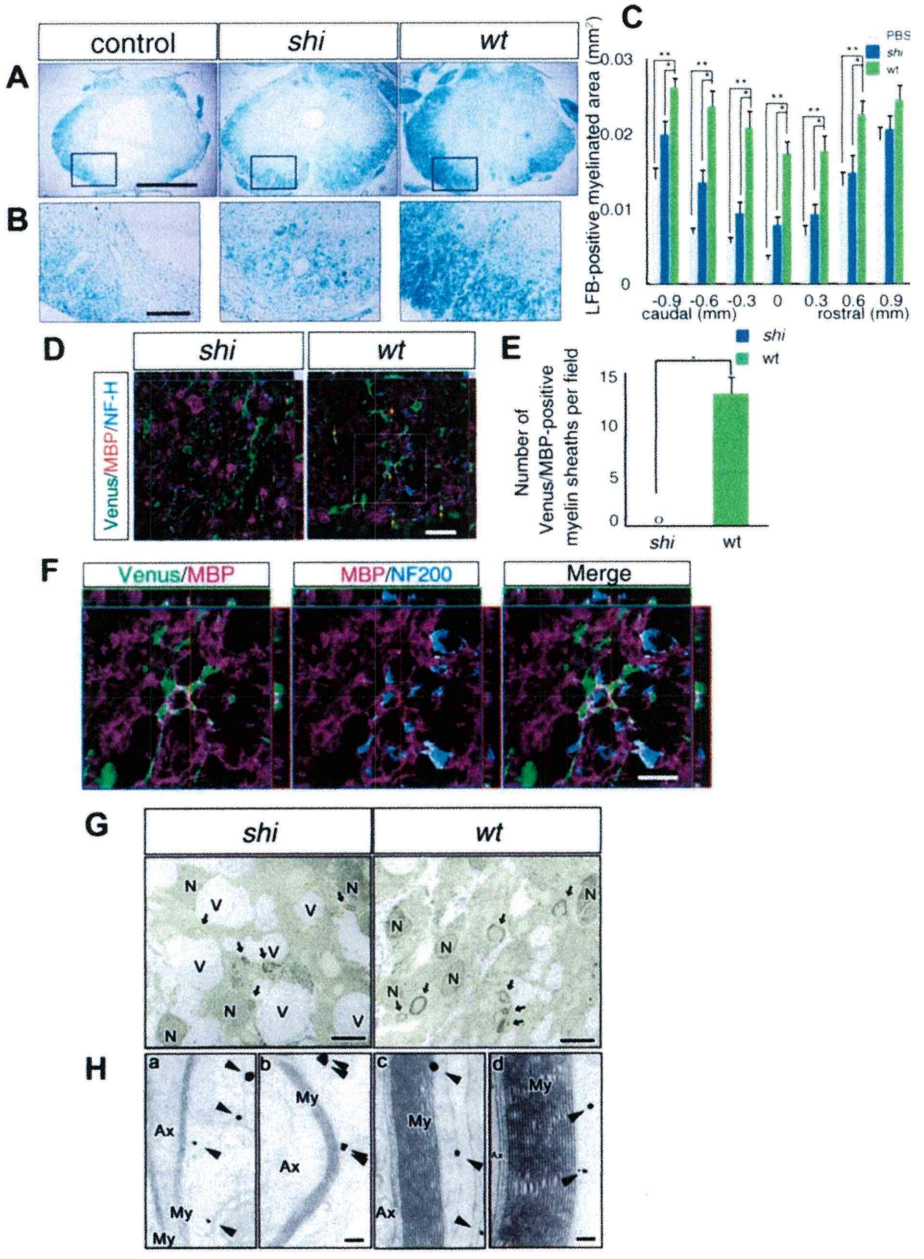


**Figure 5.** Grafted *wt*-neural stem/progenitor cells (NS/PCs), but not *shi*-NS/PCs, preserved and/or enhanced myelination within the injured spinal cord. **(A):** Representative LFB-staining images of axially sectioned spinal cord at the lesion epicenter, 7 weeks after the injury. **(B):** Higher magnification images of the boxed areas in (A). **(C):** Quantitative analysis of the myelinated area assessed on LFB-stained axial sections revealed a greater myelinated area in the *wt*-NS/PC group, with significant differences observed at all points assayed except 0.9-mm rostral to the epicenter ($n = 4$ mice per group; *, $p < .05$, *wt*-NS/PC group vs. *shi*-NS/PC group; **, $p < .05$, *wt*-NS/PC group vs. control). **(D):** Representative immunohistochemical images stained for Venus, MBP, and NF-H. In the *shi*-NS/PC group, there were no $Venus^+/MBP^+$ double-positive myelin sheaths even in areas in which myelin was rather well preserved. In the *wt*-NS/PC group, some MBP-positive myelin sheaths were also Venus positive (arrows). **(E):** Quantitative analysis of $Venus^+/MBP^+$ double-positive sheaths. There was no $Venus^+/MBP^+$ double-positive myelin sheath derived from *shi*-NS/PCs (*, $p < .01$). **(F):** Enlarged image of the boxed area in (D). *wt*-NS/PC-derived $Venus^+$ sheath was also $MBP^+$ which enwrapped the $NF\text{-}H^+$ neuronal fiber. **(G):** By immuno-electron microscopy, the transplanted cells were clearly identifiable by the black dots from the anti-green fluorescent protein (GFP) antibody. The number of $GFP^+$ grafted cells in the injured site after spinal cord injury was quite similar; however, the myelin lamellar structures were totally different between *shi*-NS/PC-derived (left) and wt-NS/PC-derived (right) grafted cells. In the cytoplasm of the grafted *shi*-NS/PC-derived cells, multiple electron-lucent vacuoles were frequently observed, but they were observed much less in the cells derived from wild-type grafts. **(H):** At high magnification, remyelinated axons could be found that were surrounded by $GFP^+$ transplanted cells (a–d). The GFP antibody labeling was often observed in the outer cytoplasm of the myelin (arrowheads). Note the huge difference in thickness of the myelin sheaths in the recipients of the *wt*-NS/PCs compared with the recipients of the *shi*-NS/PCs. Moreover, the formation of the major dense line in the newly formed myelin was selectively affected, especially in recipients of the *shi* mouse-derived grafts. Arrows: remyelinating graft cells; arrowheads: GFP immunoreactivity was indicated as black dots, yellow area: GFP-positive area, Scale bars = 500 $\mu$m in (A), 50 $\mu$m in (B), 20 $\mu$m in (D), 10 $\mu$m in (F), 5 $\mu$m in (G), 0.1 $\mu$m in (H-a, b, c, d). Abbreviations: Ax, Axon; LFB, Luxol Fast Blue; MBP, myelin basic protein; My: myelin; N, nucleus; NF-H, neurofilament-heavy chain; PBS, phosphate-buffered saline; *shi*, *shiverer*; V, vacuole; wt, wild type.

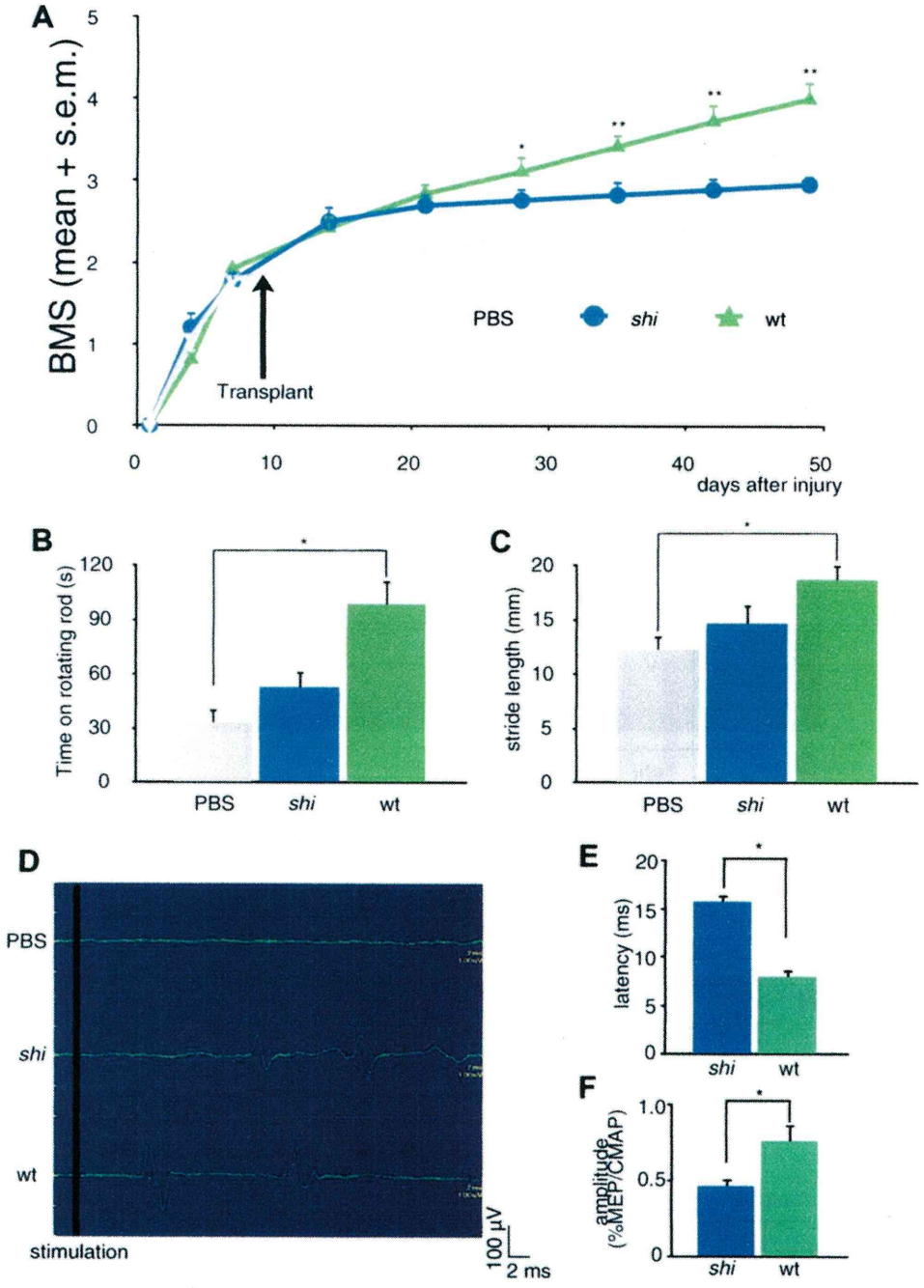


**Figure 6.** Assessment of functional recovery after spinal cord injury (SCI) and neural stem/precursor cell (NS/PC) transplantation. **(A):** Mean BMS scores for each group over the 7-week recovery period. Although there was no significant difference in the BMS scores among the control (PBS), *shi*-NS/PC, and *wt*-NS/PC groups on day 14, the *wt*-NS/PC group exhibited significantly better functional recovery than the control group on day 28 and thereafter. There was no significant difference in the BMS scores between the *shi*-NS/PC and control groups. Furthermore, the *wt*-NS/PC group showed significantly better recovery than the *shi*-NS/PC group on days 42 and 49 (control, $n = 14$; *shi*-NS/PC group, $n = 15$; *wt*-NS/PC group, $n = 13$; *, $p < .05$, *wt*-NS/PC group vs. control; **, $p < .05$, *wt*-NS/PC group vs. *shi*-NS/PC group or *wt*-NS/PCs group vs. control). **(B):** Time on the rotating rod in each group, 7 weeks after injury. The *wt*-NS/PC group stayed on the rod significantly longer than the control (PBS) group. There was no significant difference between the *shi*-NS/PC group and the control group ($n = 5$ each; *, $p < .05$). **(C):** Stride length of each group obtained by gait analysis. The *wt*-NS/PC group showed a significantly greater stride length than the control group. There was no significant difference between that of the *shi*-NS/PC group and the control (PBS) group ($n = 5$ each; *, $p < .05$). **(D):** Representative profiles of MEPs from each group evaluated 7 weeks after injury. Although MEP waves were detected in the *shi*-NS/PC and *wt*-NS/PC groups, no waves were detected in the control (PBS) group. **(E):** Latency of MEP response in the *shi*-NS/PC and *wt*-NS/PC groups. The MEP latency was significantly longer in the *shi*-NS/PC group than in the *wt*-NS/PC group ($n = 3$ each; *, $p < .05$). **(F):** MEP amplitude assessed by the MEP/CMAP ratio (%) of *shi*-NS/PC and *wt*-NS/PC groups. The *wt*-NS/PC group showed a significantly higher MEP amplitude than did the *shi*-NS/PC group ($n = 3$ each; *, $p < .05$). Abbreviations: BMS, Basso Mouse Scale; CMAP, compound motor action potential; MEP, motor-evoked potential; PBS, phosphate-buffered saline; *shi, shiverer*; wt, wild type.

without immunosuppression, their cell survival was much poorer than that of *wt*-NS/PCs derived from C57BL/6J mice. This was unexpected as the CNS is generally considered to be immune privileged. In fact, no surviving *shi*-NS/PCs were observed in the injured spinal cord of the C57BL/6J host at 5 weeks after transplantation, and no functional recovery was detected (Supporting Information Fig. 3). Thus, rather than using conventional pharmacologic immunosuppression, to minimize immunological barriers for long-term engraftment after SCI, we adopted NOD/SCID mice as hosts, which could be used as recipients even in the xenograft of human cells into SCI mice models [3, 41]. While NOD/SCID mice have neutrophils, macrophages, and microglia resulting in innate immune responses, we observed similar survival rate of *shi*-NS/PCs and *wt*-NS/PCs for all through 6 weeks and identical differentiation characteristics in the injured spinal cord. Moreover, we observed no evidence of progressive loss of either *shi*-derived or *wt*-derived cells.

Based on these grounds, by taking advantage of NOD/SCID mice as host, we investigated the role of graft-derived remyelination in functional recovery after NS/PC transplantation for SCI, which has been proposed as a possible mechanism [17, 44]. We found that the grafted NS/PCs were differentiated into oligodendrocytes and remyelinated spared axons in the injured spinal cord. Although some spontaneous remyelination by endogenous oligodendrocyte precursor cells (OPCs) is seen after SCI, the number of demyelinated axons increases in the chronic phase [45]. These observations prompted studies in which myelinating Schwann cells [46, 47], olfactory ensheathing glia [48, 49], and OPCs [50, 51] were transplanted in the hope that remyelination of the remaining axonal pathways by these cells would induce symptomatic relief after SCI. In fact, these reports showed promising results in locomotor functional recovery and histological assessments, which included evidence of graft-derived remyelination. The connection between remyelination and functional recovery, however, was not directly addressed in these reports.

Here, by using the deficient myelination in *shiverer* mutant mice, we have obtained direct evidence that remyelination by graft-derived oligodendrocytes contributes greatly to the functional recovery after SCI. Because of their genetic lack of MBP, a major component of CNS myelin, *shiverer* mutant mice have been used in numerous studies as transplant hosts for engrafted wild-type donor cells, including ESCs [52, 53], Schwann cells [54, 55], NS/PCs [56, 57], glial precursors [58], OPCs [59], and iPSC-derived NS/PCs [15], all of which produced mature myelin that was unequivocally detected by immunohistochemistry. Furthermore, a previous study on chimeric *shiverer*/wild-type mice showed that the myelination defects caused by the *shiverer* mutation are cell-autonomous, and that the myelin sheaths elaborated by *shiverer* mutant oligodendrocytes do not harm wild-type sheaths [60]. In this study, we used the *shiverer* mice not as hosts but as donors, to determine whether *shiverer* NS/PCs could promote functional recovery after SCI. To the best of our knowledge, there are no previous reports in which *shiverer* mouse cells have been used as grafts.

In this study, we first confirmed the similarity of *shi*-NS/PCs to *wt*-NS/PCs in vitro as well as in vivo. The *shi*-NS/PCs and *wt*-NS/PCs showed similar proliferation rates in vitro and survival rates within the injured spinal cord. Furthermore, the differentiation pattern of *shi*-NS/PCs was quite similar to that of *wt*-NS/PCs both in vitro and in vivo. A previous in vitro study demonstrated that OPCs derived from *shiverer* mice differentiate into mature oligodendrocytes [61]. Consistent with this, we found that *shi*-NS/PCs differentiated into $CNPase^+$ oligodendrocytes, indicating their capacity to generate a subset of myelin proteins. Furthermore, the *shi*-NS/PCs gave rise to O1 and $PLP^+$ oligodendrocytes, which are thought to represent mature cells [62, 63].

A previous in vivo study also showed that the formation of a thin myelin sheath is common in the *shiverer* CNS [64]. In *shiverer* mice, however, the CNS myelin is not uniformly compacted, and the axoglial junctions are irregular in shape, size, and distribution [65], suggesting that MBP plays a critical role in the compaction of CNS myelin. Consistent with their findings, our immuno-EM studies showed that *shi*-NS/PC-derived oligodendrocytes formed only thin and loose myelin sheaths, while *wt*-NS/PC-derived oligodendrocytes formed far more substantial myelin sheaths. At the chronic phase of SCI, some axons remain demyelinated and others have only thin myelin sheaths [66], which causes abnormal signal conduction [67]. The thinly myelinated axons in the *shi*-NS/PC group could not conduct signals very well, resulting in an increased MEP latency and a smaller amplitude in the *shi*-NS/PC group compared with the *wt*-NS/PC group. Recent studies have established MEP as a sensitive technique for recording conduction in the CNS [14, 36, 68-70]. Eftekharpour et al. [56] demonstrated a significantly shortened latency in the spinal cord-evoked potential in adult *shiverer* mice after wild-type NS/PCs transplantation, suggesting that conduction differences could be owing to spinal cord myelination, all else being equal.

In this study, we did not detect any MEP response in the control group, although even the *shi*-NS/PC-grafted animals exhibited a low-level MEP response with the longer latency and smaller amplitude (Fig. 6D, 6E). The significant difference in the latency and amplitude between *shi*-NS/PC- and *wt*-NS/PC-grafted animals indicated that nerve conduction in the spinal cord was impaired in the mutant group, which could potentially be due to faulty remyelination by the myelin-deficient graft-derived oligodendrocytes. Conversely, the current findings suggest that the transplantation of NS/PCs, regardless of their capacity to generate myelin, improves nerve conduction enough to elicit at least a minimal signal. Furthermore, the remyelination by *wt*-NS/PCs-derived oligodendrocytes shortened the MEP latency compared to remyelination by myelin-deficient oligodendrocytes, putatively by enabling saltatory conduction.

The difference in the myelinating capacity of the *wt*- and *shi*-NS/PC-derived oligodendrocytes also affected the myelinated area of the injured spinal cord. The increase in the $LFB^+$ myelinated area in the *wt*-NS/PC group may be attributable to remyelination as well as the prevention of demyelination. In fact, the transplantation of *shi*-NS/PCs also enlarged the $LFB^+$ area, primarily by preventing demyelination, and resulted in the functional improvement observed in the early time points after transplantation in the *shi*-NS/PC group, as in the *wt*-NS/PC group.

Some studies have reported that the application of growth factors prevents demyelination after SCI [71, 72]. Functional recovery was observed soon after the treatment in those studies and this one, suggesting that trophic factors cause functional recovery early in the post-transplantation period. In fact, we confirmed that the *shi*-NS/PCs expressed mRNAs for many trophic factors, at levels that were almost identical to those of *wt*-NS/PCs (Supporting Information Fig. 4). Among these, the mRNAs encoding CNTF, growth and differentiation factor (GDF11), PDGF A (PDGFA), and vascular endothelial growth factor B showed relatively high expression levels. Other reports that discuss cell transplantation approaches for the treatment of SCI have emphasized the significance of trophic factors secreted by the grafted cells [73]. It is possible that trophic support provided by the grafts prevents demyelination and promotes functional recovery, although our finding that the growth factor mRNAs levels were almost the same in *wt*- and

*shi*-neurospheres suggests that they probably have only a partial effect, if any. Although other studies have suggested that graft-derived neurons [33, 74] and astrocytes [1] are important for functional recovery, similar percentages of the various cell types were generated by the *wt*- and *shi*-NS/PCs in this study.

## Conclusion

We demonstrated that grafted NS/PCs-derived remyelination contributed to functional recovery after SCI. As myelination is a predominant contribution of grafted NS/PCs, NS/PCs can clearly target the myelination/demyelination issue and thus NS/PCs indeed hold promise for SCI treatment. Here, we elucidated one of the mechanisms that contribute to the efficacy of transplanting NS/PCs for SCI. Further comparisons of NS/PC and OPC transplantations will be needed before they can be used clinically. While not required by the Food and Drug Administration, we and others in the field believe that unraveling the regenerative mechanisms piece by piece is the quickest way to develop clinical approaches for the repair of SCI.

## Acknowledgments

We thank Drs. Kunihiko Suzuki, Kinuko Suzuki, and Aileen Anderson for their critical comments on the manuscript; Tokuko Harada for tender animal care; Sachiyo Miyao and Hiroko Shimada for technical support; and Dr. Hiroko Baba (Tokyo University of Pharmacy and Life Science) for the kind gift of the *shiverer* mice. This work was supported by grants from the Program for the Promotion of Fundamental Studies in Health Sciences of the National Institute of Biomedical Innovation (NIBIO); a grant from the Uehara Memorial Foundation; Grants-in-Aid for Scientific Research from the Japan Society for the Promotion of Science (JSPS) and the Ministry of Education, Culture, Sports, Science and Technology of Japan (MEXT); the Project for the Realization of Regenerative Medicine and support for the core institutes for iPSC research from MEXT; the "Funding Program for World-leading Innovative R&D on Science and Technology" to H.O. from the Ministry of Health, Labor, and Welfare; the General Insurance Association of Japan; Research Fellowships for Young Scientists from the Japan Society for the Promotion of Science; Keio Gijuku Academic Development Funds; and a Grant-in-aid for the Global COE program from MEXT to Keio University.

## Disclosure of Potential Conflicts of Interest

The authors indicate no potential conflicts of interest.

## References

1 Hofstetter CP, Schwarz EJ, Hess D et al. Marrow stromal cells form guiding strands in the injured spinal cord and promote recovery. Proc Natl Acad Sci USA 2002;99:2199–2204.
2 Cao Q, Xu XM, Devries WH et al. Functional recovery in traumatic spinal cord injury after transplantation of multineurotrophin-expressing glial-restricted precursor cells. J Neurosci 2005;25:6947–6957.
3 Cummings BJ, Uchida N, Tamaki SJ et al. Human neural stem cells differentiate and promote locomotor recovery in spinal cord-injured mice. Proc Natl Acad Sci USA 2005;102:14069–14074.
4 Keirstead HS, Nistor G, Bernal G et al. Human embryonic stem cell-derived oligodendrocyte progenitor cell transplants remyelinate and restore locomotion after spinal cord injury. J Neurosci 2005;25: 4694–4705.
5 Karimi-Abdolrezaee S, Eftekharpour E, Wang J et al. Delayed transplantation of adult neural precursor cells promotes remyelination and functional neurological recovery after spinal cord injury. J Neurosci 2006;26:3377–3389.
6 Salazar DL, Uchida N, Hamers FP et al. Human neural stem cells differentiate and promote locomotor recovery in an early chronic spinal cord injury NOD-scid mouse model. PLoS ONE 2010;5:e12272.
7 Ogawa Y, Sawamoto K, Miyata T et al. Transplantation of in vitro-expanded fetal neural progenitor cells results in neurogenesis and functional recovery after spinal cord contusion injury in adult rats. J Neurosci Res 2002;69:925–933.
8 Hofstetter CP, Holmstrom NA, Lilja JA et al. Allodynia limits the usefulness of intraspinal neural stem cell grafts; directed differentiation improves outcome. Nat Neurosci 2005;8:346–353.
9 Iwanami A, Kaneko S, Nakamura M et al. Transplantation of human neural stem cells for spinal cord injury in primates. J Neurosci Res 2005;80:182–190.
10 Moreno-Manzano V, Rodriguez-Jimenez FJ, Garcia-Rosello M et al. Activated spinal cord ependymal stem cells rescue neurological function. Stem Cells 2009;27:733–743.
11 McDonald JW, Liu XZ, Qu Y et al. Transplanted embryonic stem cells survive, differentiate and promote recovery in injured rat spinal cord. Nat Med 1999;5:1410–1412.
12 Kumagai G, Okada Y, Yamane J et al. Roles of ES cell-derived gliogenic neural stem/progenitor cells in functional recovery after spinal cord injury. PLoS ONE 2009;4:e7706.
13 Chen J, Bernreuther C, Dihne M et al. Cell adhesion molecule l1-transfected embryonic stem cells with enhanced survival support regrowth of corticospinal tract axons in mice after spinal cord injury. J Neurotrauma 2005;22:896–906.
14 Erceg S, Ronaghi M, Oria M et al. Transplanted oligodendrocytes and motoneuron progenitors generated from human embryonic stem cells promote locomotor recovery after spinal cord transection. Stem Cells 2010;28:1541–1549.
15 Tsuji O, Miura K, Okada Y et al. Therapeutic potential of appropriately evaluated safe-induced pluripotent stem cells for spinal cord injury. Proc Natl Acad Sci USA 2010;107:12704–12709.
16 Nori S, Okada Y, Yasuda A et al. Grafted human-induced pluripotent stem-cell-derived neurospheres promote motor functional recovery after spinal cord injury in mice. Proc Natl Acad Sci USA 2011;108: 16825–16830.
17 Barnabe-Heider F, Frisen J. Stem cells for spinal cord repair. Cell Stem Cell 2008;3:16–24.
18 Lindvall O, Kokaia Z. Stem cells in human neurodegenerative disorders–time for clinical translation? J Clin Invest 2010;120:29–40.
19 Bird TD, Farrell DF, Sumi SM. Brain lipid composition of the shiverer mouse: (genetic defect in myelin development). J Neurochem 1978;31:387–391.
20 Dupouey P, Jacque C, Bourre JM et al. Immunochemical studies of myelin basic protein in shiverer mouse devoid of major dense line of myelin. Neurosci Lett 1979;12:113–118.
21 Privat A, Jacque C, Bourre JM et al. Absence of the major dense line in myelin of the mutant mouse "shiverer". Neurosci Lett 1979;12: 107–112.
22 Roach A, Boylan K, Horvath S et al. Characterization of cloned cDNA representing rat myelin basic protein: Absence of expression in brain of shiverer mutant mice. Cell 1983;34:799–806.
23 Kimura M, Inoko H, Katsuki M et al. Molecular genetic analysis of myelin-deficient mice: Shiverer mutant mice show deletion in gene (s) coding for myelin basic protein. J Neurochem 1985;44:692–696.
24 Roach A, Takahashi N, Pravtcheva D et al. Chromosomal mapping of mouse myelin basic protein gene and structure and transcription of the partially deleted gene in shiverer mutant mice. Cell 1985;42:149–155.
25 Mikoshiba K, Okano H, Tamura T et al. Structure and function of myelin protein genes. Annu Rev Neurosci 1991;14:201–217.
26 Reynolds BA, Tetzlaff W, Weiss S. A multipotent EGF-responsive striatal embryonic progenitor cell produces neurons and astrocytes. J Neurosci 1992;12:4565–4574.
27 Stankoff B, Aigrot MS, Noel F et al. Ciliary neurotrophic factor (CNTF) enhances myelin formation: A novel role for CNTF and CNTF-related molecules. J Neurosci 2002;22:9221–9227.
28 Kanemura Y, Mori H, Kobayashi S et al. Evaluation of in vitro proliferative activity of human fetal neural stem/progenitor cells using

indirect measurements of viable cells based on cellular metabolic activity. J Neurosci Res 2002;69:869–879.
29 Yamane J, Nakamura M, Iwanami A et al. Transplantation of galectin-1-expressing human neural stem cells into the injured spinal cord of adult common marmosets. J Neurosci Res 2010;88:1394–1405.
30 Stirling DP, Liu S, Kubes P et al. Depletion of Ly6G/Gr-1 leukocytes after spinal cord injury in mice alters wound healing and worsens neurological outcome. J Neurosci 2009;29:753–764.
31 Okada S, Ishii K, Yamane J et al. In vivo imaging of engrafted neural stem cells: Its application in evaluating the optimal timing of transplantation for spinal cord injury. FASEB J 2005;19:1839–1841.
32 Takahashi Y, Tsuji O, Kumagai G et al. Comparative study of methods for administering neural stem/progenitor cells to treat spinal cord injury in mice. Cell Transplant 2011;205:727–739.
33 Abematsu M, Tsujimura K, Yamano M et al. Neurons derived from transplanted neural stem cells restore disrupted neuronal circuitry in a mouse model of spinal cord injury. J Clin Invest 2010;120:3255–3266.
34 Basso DM, Fisher LC, Anderson AJ et al. Basso Mouse Scale for locomotion detects differences in recovery after spinal cord injury in five common mouse strains. J Neurotrauma 2006;23:635–659.
35 Ogura H, Matsumoto M, Mikoshiba K. Motor discoordination in mutant mice heterozygous for the type 1 inositol 1,4,5-trisphosphate receptor. Behav Brain Res 2001;122:215–219.
36 Oria M, Chatauret N, Raguer N et al. A new method for measuring motor evoked potentials in the awake rat: Effects of anesthetics. J Neurotrauma 2008;25:266–275.
37 Reynolds BA, Rietze RL. Neural stem cells and neurospheres—re-evaluating the relationship. Nat Methods 2005;2:333–336.
38 Kim JE, Liu BP, Park JH et al. Nogo-66 receptor prevents raphespinal and rubrospinal axon regeneration and limits functional recovery from spinal cord injury. Neuron 2004;44:439–451.
39 Kaneko S, Iwanami A, Nakamura M et al. A selective Sema3A inhibitor enhances regenerative responses and functional recovery of the injured spinal cord. Nat Med 2006;12:1380–1389.
40 Murray KC, Nakae A, Stephens MJ et al. Recovery of motoneuron and locomotor function after spinal cord injury depends on constitutive activity in 5-HT2C receptors. Nat Med 2010;16:694–700.
41 Anderson AJ, Haus DL, Hooshmand MJ et al. Achieving stable human stem cell engraftment and survival in the CNS: Is the future of regenerative medicine immunodeficient? Regen Med 2011;6:367–406.
42 Shultz LD, Schweitzer PA, Christianson SW et al. Multiple defects in innate and adaptive immunologic function in NOD/LtSz-scid mice. J Immunol 1995;154:180–191.
43 Greiner DL, Hesselton RA, Shultz LD. SCID mouse models of human stem cell engraftment. Stem Cells 1998;16:166–177.
44 Okano H. Neural stem cells: Progression of basic research and perspective for clinical application. Keio J Med 2002;51:115–128.
45 Totoiu MO, Keirstead HS. Spinal cord injury is accompanied by chronic progressive demyelination. J Comp Neurol 2005;486:373–383.
46 Kuhlengel KR, Bunge MB, Bunge RP. Implantation of cultured sensory neurons and Schwann cells into lesioned neonatal rat spinal cord. I. Methods for preparing implants from dissociated cells. J Comp Neurol 1990;293:63–73.
47 Martin D, Schoenen J, Delree P et al. Grafts of syngenic cultured, adult dorsal root ganglion-derived Schwann cells to the injured spinal cord of adult rats: Preliminary morphological studies. Neurosci Lett 1991;124:44–48.
48 Li Y, Field PM, Raisman G. Repair of adult rat corticospinal tract by transplants of olfactory ensheathing cells. Science 1997;277:2000–2002.
49 Imaizumi T, Lankford KL, Kocsis JD. Transplantation of olfactory ensheathing cells or Schwann cells restores rapid and secure conduction across the transected spinal cord. Brain Res 2000;854:70–78.
50 Bambakidis NC, Miller RH. Transplantation of oligodendrocyte precursors and sonic hedgehog results in improved function and white matter sparing in the spinal cords of adult rats after contusion. Spine J 2004;4:16–26.
51 Cao Q, He Q, Wang Y et al. Transplantation of ciliary neurotrophic factor-expressing adult oligodendrocyte precursor cells promotes remyelination and functional recovery after spinal cord injury. J Neurosci 2010;30:2989–3001.
52 Liu S, Qu Y, Stewart TJ et al. Embryonic stem cells differentiate into oligodendrocytes and myelinate in culture and after spinal cord transplantation. Proc Natl Acad Sci USA 2000;97:6126–6131.
53 Low HP, Greco B, Tanahashi Y et al. Embryonic stem cell rescue of tremor and ataxia in myelin-deficient shiverer mice. J Neurol Sci 2009;276:133–137.
54 Baron-Van Evercooren A, Gansmuller A, Duhamel E et al. Repair of a myelin lesion by Schwann cells transplanted in the adult mouse spinal cord. J Neuroimmunol 1992;40:235–242.
55 McKenzie IA, Biernaskie J, Toma JG et al. Skin-derived precursors generate myelinating Schwann cells for the injured and dysmyelinated nervous system. J Neurosci 2006;26:6651–6660.
56 Eftekharpour E, Karimi-Abdolrezaee S, Wang J et al. Myelination of congenitally dysmyelinated spinal cord axons by adult neural precursor cells results in formation of nodes of Ranvier and improved axonal conduction. J Neurosci 2007;27:3416–3428.
57 Mothe AJ, Tator CH. Transplanted neural stem/progenitor cells generate myelinating oligodendrocytes and Schwann cells in spinal cord demyelination and dysmyelination. Exp Neurol 2008;213:176–190.
58 Windrem MS, Schanz SJ, Guo M et al. Neonatal chimerization with human glial progenitor cells can both remyelinate and rescue the otherwise lethally hypomyelinated shiverer mouse. Cell Stem Cell 2008;2:553–565.
59 Windrem MS, Nunes MC, Rashbaum WK et al. Fetal and adult human oligodendrocyte progenitor cell isolates myelinate the congenitally dysmyelinated brain. Nat Med 2004;10:93–97.
60 Mikoshiba K, Yokoyama M, Takamatsu K et al. Chimeric analysis of the pathogenesis of dysmyelination of shiverer mutant mice. Presence of patches of MBP-positive and negative sites in white matter indicating the absence of humoral factors for dysmyelination. Dev Neurosci 1982;5:520–524.
61 Seiwa C, Kojima-Aikawa K, Matsumoto I et al. CNS myelinogenesis in vitro: Myelin basic protein deficient shiverer oligodendrocytes. J Neurosci Res 2002;69:305–317.
62 Okano H, Miura M, Moriguchi A et al. Inefficient transcription of the myelin basic protein gene possibly causes hypomyelination in myelin-deficient mutant mice. J Neurochem 1987;48:470–476.
63 McDonald JW, Belegu V. Demyelination and remyelination after spinal cord injury. J Neurotrauma 2006;23:345–359.
64 Rosenbluth J. Central myelin in the mouse mutant shiverer. J Comp Neurol 1980;194:639–648.
65 Inoue Y, Nakamura R, Mikoshiba K et al. Fine structure of the central myelin sheath in the myelin deficient mutant Shiverer mouse, with special reference to the pattern of myelin formation by oligodendroglia. Brain Res 1981;219:85–94.
66 Griffiths IR, McCulloch MC. Nerve fibres in spinal cord impact injuries. Part 1. Changes in the myelin sheath during the initial 5 weeks. J Neurol Sci 1983;58:335–349.
67 Nashmi R, Fehlings MG. Changes in axonal physiology and morphology after chronic compressive injury of the rat thoracic spinal cord. Neuroscience 2001;104:235–251.
68 Pluchino S, Quattrini A, Brambilla E et al. Injection of adult neurospheres induces recovery in a chronic model of multiple sclerosis. Nature 2003;422:688–694.
69 Biffi A, De Palma M, Quattrini A et al. Correction of metachromatic leukodystrophy in the mouse model by transplantation of genetically modified hematopoietic stem cells. J Clin Invest 2004;113:1118–1129.
70 Ito Z, Sakamoto K, Imagama S et al. *N*-Acetylglucosamine 6-*O*-sulfotransferase-1-deficient mice show better functional recovery after spinal cord injury. J Neurosci 2010;30:5937–5947.
71 Jakeman LB, Wei P, Guan Z et al. Brain-derived neurotrophic factor stimulates hindlimb stepping and sprouting of cholinergic fibers after spinal cord injury. Exp Neurol 1998;154:170–184.
72 Kitamura K, Iwanami A, Nakamura M et al. Hepatocyte growth factor promotes endogenous repair and functional recovery after spinal cord injury. J Neurosci Res 2007;85:2332–2342.
73 Sharp J, Frame J, Siegenthaler M et al. Human embryonic stem cell-derived oligodendrocyte progenitor cell transplants improve recovery after cervical spinal cord injury. Stem Cells 2010;28:152–163.
74 Courtine G, Gerasimenko Y, van den Brand R et al. Transformation of nonfunctional spinal circuits into functional states after the loss of brain input. Nat Neurosci 2009;12:1333–1342.

**See www.StemCells.com for supporting information available online.**

# Grafted human-induced pluripotent stem-cell–derived neurospheres promote motor functional recovery after spinal cord injury in mice

Satoshi Nori[a,b,1], Yohei Okada[a,c,1], Akimasa Yasuda[a,b], Osahiko Tsuji[b], Yuichiro Takahashi[a,b], Yoshiomi Kobayashi[a,b], Kanehiro Fujiyoshi[b], Masato Koike[d], Yasuo Uchiyama[d], Eiji Ikeda[e,f], Yoshiaki Toyama[b], Shinya Yamanaka[g], Masaya Nakamura[b,2], and Hideyuki Okano[a,2]

[a]Department of Physiology, [b]Department of Orthopaedic Surgery, [c]Kanrinmaru-Project, School of Medicine, Keio University, Shinjuku, Tokyo 160-8582, Japan; [d]Department of Cell Biology and Neuroscience, Juntendo University Graduate School of Medicine, Bunkyoku, Tokyo 113-8421, Japan; [e]Department of Pathology, School of Medicine, Keio University, Shinjuku, Tokyo 160-8582, Japan; [f]Department of Pathology, Yamaguchi University Graduate School of Medicine, Ube, Yamaguchi 755-8505, Japan; and [g]Center for iPS Cell Research and Application, Kyoto University, Shogoin, Sakyoku, Kyoto 606-8507, Japan

Edited by Fred H. Gage, The Salk Institute, San Diego, CA, and approved September 1, 2011 (received for review May 20, 2011)

**Once their safety is confirmed, human-induced pluripotent stem cells (hiPSCs), which do not entail ethical concerns, may become a preferred cell source for regenerative medicine. Here, we investigated the therapeutic potential of transplanting hiPSC-derived neurospheres (hiPSC-NSs) into nonobese diabetic (NOD)-severe combined immunodeficient (SCID) mice to treat spinal cord injury (SCI). For this, we used a hiPSC clone (201B7), established by transducing four reprogramming factors (Oct3/4, Sox2, Klf4, and c-Myc) into adult human fibroblasts. Grafted hiPSC-NSs survived, migrated, and differentiated into the three major neural lineages (neurons, astrocytes, and oligodendrocytes) within the injured spinal cord. They showed both cell-autonomous and noncell-autonomous (trophic) effects, including synapse formation between hiPSC-NS–derived neurons and host mouse neurons, expression of neurotrophic factors, angiogenesis, axonal regrowth, and increased amounts of myelin in the injured area. These positive effects resulted in significantly better functional recovery compared with vehicle-treated control animals, and the recovery persisted through the end of the observation period, 112 d post-SCI. No tumor formation was observed in the hiPSC-NS–grafted mice. These findings suggest that hiPSCs give rise to neural stem/progenitor cells that support improved function post-SCI and are a promising cell source for its treatment.**

stem-cell–based medicine | cell transplantation | neurotrauma | synaptic connection

Stem-cell–based approaches, such as the transplantation of neural stem/progenitor cells (NS/PCs), are promising sources of therapies for various central nervous system disorders (1–3). Previous studies reported functional recovery after transplantation of NS/PCs into the injured spinal cord of rodents and nonhuman primates (4–9). Furthermore, recent studies revealed that embryonic stem cells (ESCs) can generate neural cells including NS/PCs (10–12) and oligodendrocyte precursor cells (OPCs) (13, 14). Therefore, human ESC-based therapies are moving out of the laboratory and into clinical treatments for spinal cord injury (SCI) (12, 13, 15). However, the use of human ESC-based therapies is complicated by ethical concerns in certain countries. To avoid the problems associated with ESCs, we previously established induced pluripotent stem cells (iPSCs) from mouse fibroblasts (16, 17) and confirmed the therapeutic potential of iPSC-derived neurospheres (iPSC-NSs) for treating SCI in animal models (18).

Here, aiming at human iPSC-based therapies for SCI patients, we examined the therapeutic potential of human iPSC-NSs by transplanting them into nonobese diabetic severe combined immunodeficient (NOD-SCID) SCI model mice. We used a clone from human iPSCs (hiPSCs) that we established from adult human dermal fibroblasts by the retroviral transduction of four reprogramming factors; for the clone used in this study, 201B7, the factors were Oct3/4, Sox2, Klf4, and c-Myc (19). These grafted hiPSC-NSs survived, migrated, and differentiated into the three neural lineages in the injured spinal cord. They promoted angiogenesis and axonal regrowth and preserved myelination, and some formed synapses with host mouse neurons. These positive effects promoted functional recovery that persisted for up to 112 d after SCI, without tumor formation.

These findings indicated that neurospheres derived from hiPSCs are a potential cell source for transplantation therapy for SCI.

## Results

**Grafted hiPSC-NSs Survived, Migrated, and Differentiated into Three Neural Lineages.** Contusive SCI was induced at the Th10 level in NOD-SCID mice, and $5 \times 10^5$ Venus$^+$ hiPSC-NSs or PBS was injected into the lesion epicenter, 9 d after injury. To examine the effects of grafted hiPSC-NSs in the injured spinal cord, histological analyses were performed 56 d after SCI [after functional recovery, based on the Basso mouse scale (BMS) score, was observed to plateau]. Ten mice in each group were killed on day 56, and 18 mice grafted with hiPSC-NSs and 16 PBS-injected mice remained. These mice were assessed by BMS and for long-term safety of the grafted hiPSC-NSs, 112 d after SCI (Table S1).

On day 56, the grafted hiPSC-NSs had survived and migrated into the host spinal cord (Fig. 1 *A* and *B*). To examine their differentiation potentials, we performed immunohistochemical analyses and quantified the proportion of Venus$^+$ cells immunopositive for cell-type–specific markers. The engrafted hiPSC-NSs differentiated into neuronal nuclei (NeuN)$^+$ and β-tubulin isotype III (βIII tubulin)$^+$ neurons, glial fibrillary acidic protein (GFAP)$^+$ astrocytes, and adenomatous polyposis coli CC-1 (APC)$^+$ oligodendrocytes (Fig. 1 *C–F*). The βIII tubulin$^+$/Venus$^+$ neurons comprised 49.1 ± 2.0% of the Venus$^+$ cells, and the mature NeuN$^+$/Venus$^+$ neurons comprised 22.9 ± 1.0%. Thus, 56 d after SCI, about 50% of the grafted hiPSC-NSs had differentiated into neurons, about half of which were mature neurons. GFAP$^+$/Venus$^+$ astrocytes comprised 17.0 ± 1.2%, but APC$^+$/Venus$^+$ oligodendrocytes were rare (3.0 ± 0.4%). Nestin$^+$/Venus$^+$ NS/PCs made up 10.7 ± 2.2% of the total (Fig. 1*G*).

Author contributions: Y.U., Y. Toyama, S.Y., M.N., and H.O. designed research; S.N., Y.O., A.Y., O.T., Y. Takahashi, Y.K., K.F., M.K., and E.I. performed research; S.N., M.K., and E.I. analyzed data; and S.N., Y.O., M.K., M.N., and H.O. wrote the paper.

The authors declare no conflict of interest.

This article is a PNAS Direct Submission.

Freely available online through the PNAS open access option.

[1]S.N. and Y.O. contributed equally to this work.

[2]To whom correspondence may be addressed. E-mail: hidokano@a2.keio.jp or masa@sc.itc.keio.ac.jp.

This article contains supporting information online at www.pnas.org/lookup/suppl/doi:10.1073/pnas.1108077108/-/DCSupplemental.

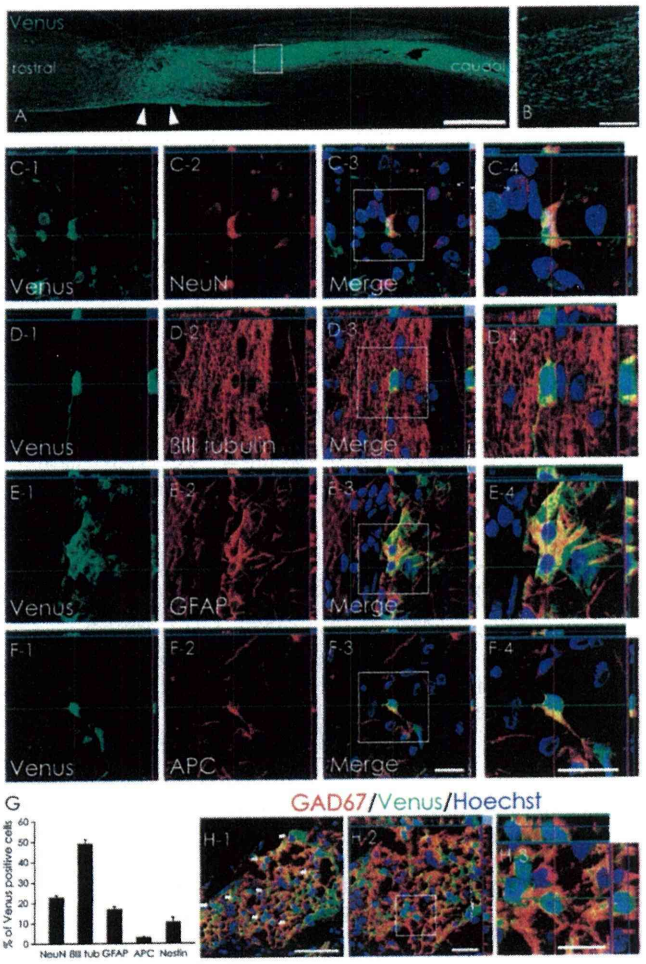


**Fig. 1.** In vivo differentiation of hiPSC-NSs. (*A* and *B*) Venus$^+$ hiPSC-NSs were integrated at or near the lesion epicenter (arrowheads). (Scale bars, 1000 μm in *A*; 100 μm in *B*.) (*C–F*) Representative images of Venus$^+$-grafted cells labeled with the neural markers NeuN$^+$ (mature neurons) (*C*); βIII tubulin$^+$ (all neurons) (*D*); GFAP$^+$ astrocytes (*E*); and APC$^+$ oligodendrocytes (*F*). (Scale bar, 20 μm.) (*G*) Percentages of cell-type–specific marker-positive cells among the Venus$^+$-grafted cells 56 d after SCI. Values are means ± SEM ($n$ = 4). (*H*) Most hiPSC-derived neurons differentiated into GAD67$^+$ (GABAergic) neurons. (Scale bars, 50 μm in *H-1*; 20 μm in *H-2*; and 10 μm in *H-3*.)

Because 22.9% of the hiPSC-NSs differentiated into mature neurons, we next examined their neurotransmitter phenotype, using neurotransmitter-specific markers. Of the Venus$^+$ cells, 15.8 ± 2% were glutamic acid decarboxylase 67 (GAD67)$^+$, indicating that 69% (15.8/22.9% = 69.0%) of the hiPSC-NS–derived mature neurons were GABAergic (Fig. 1*H*). We also found small numbers of Venus$^+$ tyrosine hydroxylase (TH)$^+$ neurons and choline acetyltransferase (ChAT)$^+$ cholinergic neurons (Fig. S1 *A* and *B*).

**Synapse Formation Between hiPSC-Derived Neurons and Host Mouse Neurons.** To evaluate the ability of the hiPSC-NS–derived neurons to integrate with the host neural circuitry, triple immunostaining was performed with antibodies to human nuclear protein (HNu), βIII tubulin, and the presynaptic protein Bassoon (Bsn). The anti-Bsn antibody is a monoclonal that selectively recognizes mouse and rat, but not human epitopes. Grafted βIII tubulin$^+$/HNu$^+$ cells in the neural parenchyma were observed in contact with the synaptic boutons of host neurons (Fig. 2*A*). In addition, triple immunostaining for HNu, βIII tubulin, and human-specific synaptophysin (hSyn) revealed dense fields of

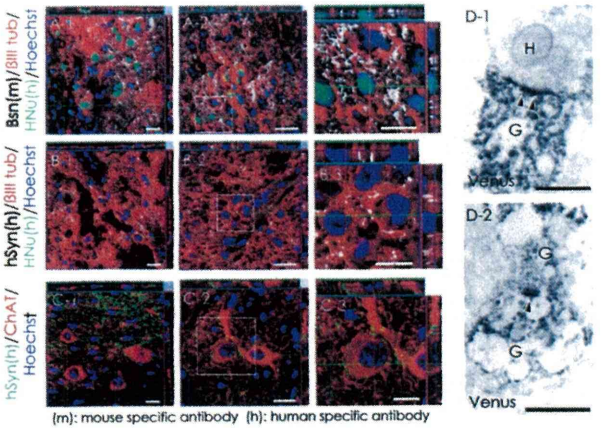


**Fig. 2.** Evidence for synapse formation between hiPSC-derived neurons and host mouse spinal cord neurons. (*A*) Sections were triple-stained with HNu (green), βIII tubulin (red), and the presynaptic marker Bassoon (Bsn, white). The Bsn antibody used here recognized the rat and mouse, but not human, protein. (*B*) Sections triple-stained for HNu (green), βIII tubulin (red), and the human-specific presynaptic marker hSyn (white). (*C*) Confocal images showing a large number of somatic and dendritic terminals from graft-derived nerve cells on host motor neurons at the ventral horns. (*D*) Electron microscopy showing synapse formation between host mouse neurons and graft-derived Venus$^+$ (black) human neurons: the pre- and postsynaptic structures indicated transmission from a host neuron to a graft-derived neuron (*D-1*) and from a graft-derived neuron to a graft-derived neuron (*D-2*). H, host neuron; G, graft-derived neuron; arrowheads, postsynaptic density. (Scale bars, 20 μm in *A-1*, *A-2*, *B-1*, *B-2*, *C-1*, and *C-2*; 10 μm in *A-3*, *B-3*, and *C-3*; and 0.5 μm in *D*.)

boutons apposed to βIII tubulin$^+$/HNu$^-$ host mouse neurons (Fig. 2*B*). These host neurons in the ventral gray matter were ChAT$^+$, and some of the boutons represented graft-specific terminals (Fig. 2*C*). Immunoelectron microscopy revealed Venus$^+$ (i.e., human) presynaptic and postsynaptic structures and synapses between host mouse neurons and Venus$^+$ hiPSC-derived neurons at the injured site (Fig. 2*D*).

**Transplantation of hiPSC-NSs Enhanced Angiogenesis and Axonal Regrowth but Did Not Induce Abnormal Innervation of Pain-Related CGRP$^+$ Afferents After SCI.** To evaluate the effects of hiPSC-NS transplantation on angiogenesis after SCI, immunohistochemical analyses for platelet endothelial cell adhesion molecule-1 (PECAM-1) were performed. There were significantly more PECAM-1$^+$ blood vessels at the lesion epicenter in the hiPSC-NS group than in the control group (Fig. 3 *A–C*). To determine the source of the angiogenic signals, we examined the vascular endothelial growth factor (VEGF) expression in the grafted spinal cord by immunohistochemistry (Fig. 3*D*). Quantitative analyses revealed that the VEGF$^+$ area at the lesion epicenter was significantly larger in the hiPSC-NS group than in the control group (Fig. 3*E*). Furthermore, both GFAP$^+$/Venus$^+$ hiPSC-derived astrocytes (Fig. 3*F*) and GFAP$^+$/Venus$^-$ host mouse astrocytes expressed VEGF (Fig. 3*G*), consistent with the results of RT-PCR (Fig. 3 *H* and *I*). Note that the mouse *Vegf* mRNA expression level was higher in the hiPSC-NS–grafted mice than in PBS-injected mice.

Because angiogenesis generally improves tissue sparing, we examined the atrophic changes of the injured spinal cord by hematoxylin–eosin (H&E) staining. Unlike the hiPSC-NS group, atrophic changes of the injured spinal cord were prominent in the control group (Fig. 3 *J* and *K*). Quantitative analysis revealed significant differences in the transverse area of the spinal cord between the control and hiPSC-NS group, suggesting that the hiPSC-NS transplantation prevented atrophy of the injured spinal cord (Fig. 3*L*). Luxol fast blue (LFB) staining also revealed